Chemical Geology 654 (2024) 122053

Contents lists available at ScienceDirect

Chemical Geology

journal homepage: www.elsevier.com/locate/chemgeo

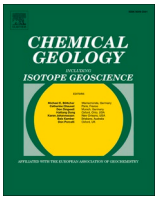

Geochemical proxies for deep-sea temperature and nutrient content in cold-water bamboo corals

Thomas J. Williams [a,*], Christopher D. Standish [a], Philippe Archambault [b], Jasmin A. Godbold [a], Martin Solan [a], Orestis L. Katsamenis [c], Philip J. Basford [c], Gavin L. Foster [a]

[a] School of Ocean and Earth Science, National Oceanography Centre Southampton, University of Southampton, Waterfront Campus, European Way, Southampton SO14 3ZH, UK
[b] ArcticNet, Québec Océan, Takuvik Joint International Laboratory CNRS, Université Laval, Quebec City, QC, Canada
[c] μ-VIS X-ray Imaging Centre, Building 5, University of Southampton, Highfield Campus, Southampton SO17 1BJ, UK

ARTICLE INFO

Editor: Michael E. Boettcher

Keywords:
Paleoclimatology
High-Mg calcites
Bamboo coral
Inter-colony variability
Intra-individual variability
Cold-water corals
Geochemistry

ABSTRACT

The impact of warming, acidification, and deoxygenation on deep-sea environments is a growing concern. Historical records are sparse, particularly at high latitudes, making climate change projections challenging. Indirect proxies, such as trace element composition of marine carbonates, such as coral skeletons, can offer an alternative method to fill data gaps but have not been realised. Here, using Laser Ablation Triple-Quadrupole Inductively Coupled Plasma Mass Spectrometry (LA-QQQ-ICP-MS), we examined micrometre-scale element variation within and between individual colonies of the bamboo coral *Keratoisis* sp. obtained from the Eastern Canadian Arctic. These data are used to assess the influence of biological variability on geochemical tracers for reconstructing past environmental conditions (temperature: Mg/Ca, Li/Mg, Sr/Ca, Ba/Ca, U/Ca; $[Ba]_{SW}$: Ba/Ca). We place these data into context, based on a survey of literature data, using refined calibrations for high-Mg calcitic Octocorals. We find reproducible (2σ relative coefficient of variation) values of Mg/Ca (3%) and Ba/Ca (6%) along the radial growth axis of all colonies and internodes of *Keratoisis* sp., indicating that these signals are likely suitable for environmental reconstructions. After revising the available multi-taxa calibrations for Mg/Ca (0.316 ± 0.026 °C/mmol/mol, $R^2 = 0.87$, $p < 0.001$) and Ba/Ca ([Ba/Ca μmol/mol] $= 0.148 \pm 0.005$ [Ba_{SW} nmol/kg], $R^2 = 0.97$, $p < 0.001$), we show that vital effects within and among *Keratoisis* sp. colonies strongly influence reconstructed temperature and $[Ba]_{SW}$, but this can be somewhat mitigated by combining multiple internode transects from one colony into a single composite series. Despite the ontogenetic variability, all colonies reveal a gradual deep-water cooling trend since the early 21st century and synchronised, multi-year spikes in Ba/Ca (and hence $[Ba]_{SW}$) that suggest substantial and coherent barium inputs to the seafloor. Our study confirms the reliability of Mg/Ca and Ba/Ca proxies in high-Mg bamboo corals for detecting multi-annual temperature and seawater barium variations in cold-water environments, but further investigation into micro-scale element behaviour influenced by biotic processes in these corals is needed to enhance confidence in reconstructions at finer spatial and temporal resolutions. We conclude that employing empirical calibrations based on multi-taxa approaches can increase the certainty of capturing regional changes in the environment more accurately than a single species calibration, while leveraging multiple element series to account for biological-induced variability improves single colony reconstructions.

1. Introduction

High-resolution historical records of the marine environment are essential for deciphering the effects of rapid anthropogenic climate change and reducing the uncertainty of projected future conditions. The ecological repercussions of climate change for deep-sea organisms, communities and biological processes, however, remain largely unresolved, though the severe changes in temperature, oxygen, pCO_2 and export of particulate organic matter projected for the seafloor (Battaglia and Joos, 2018; Chen et al., 2017) are likely to lead to ecological destabilisation across all trophic levels and marine layers by the turn of the century (Levin and Le Bris, 2015; Sweetman et al., 2017). Despite

* Corresponding author.
E-mail address: t.williams@soton.ac.uk (T.J. Williams).

https://doi.org/10.1016/j.chemgeo.2024.122053
Received 29 July 2023; Received in revised form 14 November 2023; Accepted 17 March 2024
Available online 21 March 2024

this, insufficient spatio-temporal coverage of in-situ measurements of temperature, salinity, and biogeochemical parameters for deep waters (>200 m), particularly in polar regions (Buch et al., 2019; Smith et al., 2019), has resulted in a fragmented information landscape, limiting the construction of predictive models. Although preserved environmental information from paleo-proxies can help fill in the gaps over time and space, conventional samples such as sediment and ice cores do not have the requisite time resolution to study precise, modern-era changes.

Deep-sea corals offer an opportunity to access detailed records of localised environmental history within their skeletal geochemistry that can be sampled at sub-decadal resolution over the entire lifespan of the coral (up to several 100 years in some cases; Sherwood and Risk, 2007; Robinson et al., 2014). The more holistic understanding of anthropogenic influences within the deep benthos provided by these proxy records can improve predictions of resulting environmental changes. Previous studies demonstrate that proxy records of temperature (Smith et al., 2000; Thresher et al., 2010; Lutringer et al., 2005; Case et al., 2010; Kimball et al., 2014; Montagna et al., 2005, 2014), ocean circulation and ventilation (Adkins et al., 1998; Frank et al., 2004; Robinson et al., 2005; Sherwood et al., 2008), biological productivity and nutrient concentrations (Sherwood et al., 2005a, 2011; LaVigne et al., 2011), and the isotopic and elemental properties of seawater (Anagnostou et al., 2012; Hill et al., 2012) can all be derived from the isotopic and trace and minor elemental composition of the carbonate and organic matrices of the coral skeletal structure. Frequently used species for such reconstructions are the scleractinian cold-water corals, such as *Desmophyllum dianthus* and *Lophelia pertusa,* which can build their aragonitic skeletons in undersaturated water (Stewart et al., 2022) and inhabit depths beyond the carbonate saturation horizon (Auscavitch et al., 2020). While *D. dianthus* can be found at depths beyond 2000 m (Koslow et al., 2001), *L. pertusa* is not typically found below 500 m (Davies et al., 2008), though solitary exceptions remain (Rogers, 1999). Even so, both species are known to possess significant heterogeneities in chemical composition associated with skeletal microstructure, particularly around their centres of calcification (Anagnostou et al., 2012; Gagnon et al., 2007; Stewart et al., 2016), which can frustrate efforts to reconstruct past environments reliably (Sinclair et al., 2006).

Cold-water gorgonin Octocorals (Bayer, 1956; hereafter, bamboo coral) can also grow in seawater that is undersaturated in calcium carbonate (Geyman et al., 2019; Feely et al., 2002) but do not typically exhibit centres of calcification or similar microstructural heterogeneities (Noé and Dullo, 2006), are cosmopolitan in distribution and can be found at depths beyond 4500 m (e.g. *Echinisis persephone*; Bayer and Stefani, 1987). However, deep-sea Octocorals, in general, are some of the slowest-growing corals (Sherwood and Edinger, 2009); the biomineralization processes they use is not well understood but are presumed not to precipitate in isotopic equilibrium with seawater (Farmer et al., 2015a) and, therefore, if like other deep sea corals (Smith et al., 2000), the extent of the disequilibrium may vary widely within a particular individual. Indeed, physiological processes play a significant role in controlling microscale variations in trace and minor element compositions in coral skeletons (Chalk et al., 2021; Flöter et al., 2019), which is why many proxies in bamboo corals suggest environmental variability outside of the known limits of ambient seawater conditions (Flöter et al., 2019; Flöter, 2019). In coral paleoclimatology, explicitly evaluating the effects of intra- and inter-colony variation through the application of a multi-colony approach is a useful way of ascertaining reproducible environmentally-driven signals from ontogenetic noise (e.g. Alpert et al., 2016; Hu et al., 2018) as proxies can typically exhibit poor reproducibility between single colonies due a combination of variable vital effects related to growth/calcification rates, incorporation of organic material, and seasonality of the environmental signal (Sherwood et al., 2005b; Sinclair et al., 2011; Aranha et al., 2014), among other factors. Within the field of ecology, accounting for inter-individual variability is also a necessary approach for understanding community dynamics (Bolnick et al., 2011), functional productivity (Cianciaruso et al., 2009) and responses to global change (Pistevos et al., 2011; Schlegel et al., 2012). In terms of within individual variation, it is recognised that improved reproducibility of geochemical records could be achieved by cross-validating replicate transects on adjacent growth paths (DeLong et al., 2007; DeLong et al., 2011; Kawakubo et al., 2014). As for Octocorals that grow radially, this can be carried out across a singular internode (Sinclair et al., 2011), or by sectioning the coral at different positions along its longitudinal axis to obtain different internode sections. By aligning replicate stratigraphies with in-situ environmental data (Hu et al., 2018; Cuny-Guirriec et al., 2019; Hathorne et al., 2013), this approach ultimately enhances the accuracy of paleoenvironmental reconstruction.

In cases where long-term in-situ environmental measurements are lacking, a viable calibration alternative is to compare the nominal proxy value with the ambient conditions at the collection site of a live coral (e.g. Thresher et al., 2016). Combining multiple comparisons from various taxa, depths, and geographic locations can help identify universal proxies and serve as a basis for targeted studies in the future (Stewart et al., 2020). Still, this approach has limitations, as it overlooks any ontogenetic variability and confines lifetime response mechanisms to fluctuating environmental conditions into a single datapoint. As such, we adopt a cross-study calibration method alongside a multi-colony multi-internode micrometre-scale analysis of trace and minor element variation in deep-water bamboo corals using laser ablation approaches to holistically assess the likelihood that the observed geochemical variability is indicative of environmental change. Specifically, multidecadal-scale geochemical information of Li/Ca, Mg/Ca, Sr/Ca, U/Ca, Li/Mg and Ba/Ca were extracted from four deep-water bamboo corals belonging to the species *Keratoisis* sp. (Family *Keratoisididae*, McFadden et al., 2023; Watling et al., 2022; lifespan estimate, 100 years+, Neves et al., 2014) from a region of the Canadian Arctic that is undergoing rapid environmental change (Laidre et al., 2020; Nusbaumer et al., 2019). These tracers are regularly used as proxies in other species of bamboo coral for ambient seawater temperature (Thresher et al., 2010; Lopez Correa et al., 2011; Flöter, 2019; Flöter et al., 2019) and barium concentrations (LaVigne et al., 2011; Thresher et al., 2016; Flöter et al., 2019; Geyman et al., 2019), the latter of which exhibits a nutrient-like profile in open oceans (Chow and Goldberg, 1960) and tracks patterns of other algal nutrients (Wolgemuth and Broecker, 1970). By employing *Keratoisis* sp. as a paleoceanographic proxy in cold-water environments, we also gain insight into species' responses over extended timescales beyond the limitations of current data. Additionally, we evaluate the efficacy of *Keratoisis* sp. as indirect indicators of environmental changes in the Arctic deep-sea, as they respond to these changes in ways that can be observed and studied. By examining the dependencies of various element ratios on temperature and surrounding seawater chemistry, we expect that changes in geochemical signals across the coral's lifetime will capture long-term trends and shorter cyclic environmental variability. In cases where such correlations are absent, we anticipate that biological variability will be the dominant factor influencing any observed patterns.

2. Methodology

2.1. Sample collection

Keratoisis sp. (SubFamily *Keratoisidinae*) was collected at the Disko Fan station (67° 57.9786′ N, 59° 29.6286′ W, 889 m, 2nd August 2021) within Baffin Bay using the Sub-Atlantic® Comanche (Forum Energy Technologies™, USA) remotely operated submersible from the CCGS Amundsen (Geoffroy et al., 2021). Individual colonies of *Keratoisis* sp. were collected along the planned (~ 1 km) dive transect (see supplementary material Table S1 and Fig. S1 for geo- and timestamps) and sampled close to the basal internode (near the base of the colony).

2.2. Sample processing

External debris and fauna were removed by hand, before the *Keratoisis* sp. colonies ($n = 4$) were photographed (NIKON D3300, AF-S DX VR Nikkor 18-55 mm Lens, f/3.5–5.6G II; see supplementary material Fig. S2), sealed in Ziplock bags and placed in −20 °C for 72 h. After the initial freezing, tissue was removed from the *Keratoisis* sp. skeletons with jets of re-circulated 0.45 μm membrane-filtered seawater at 4 °C using a WaterPik™ (Johannes and Wiebe, 1970). Two separate washes of 60 to 80 ml filtered seawater were used on each internode, and 20 ml was used to rinse the remainder of the skeleton, WaterPik™ reservoir, and to flush the WaterPik™ pump. The cleaned *Keratoisis* sp. skeleton portions were then vacuum sealed in PVC tubing, sealed with Parafilm®, and transported to the National Oceanography Centre, Southampton, UK.

2.3. Hydrographic data

The environmental data and sources are provided in Table 1. To calibrate *Keratoisis* sp. element values (Li/Mg, Mg/Ca, Sr/Ca, Sr/U, U/Ca) to in-situ environment conditions, proximal deep-water temperature values at the point of sampling (Amundsen Science Data Collection, 2021) and during previous research cruises (K. Azestu-Scott, pers. comm., May 31, 2022) were obtained from in-situ measurements using a precise probe or CTD (conductivity, temperature, depth) profiles. As proximate temperature values were only available for the previous three years (2018–2021), with one value each year between June–August, these were compared to a deep-water 20th century temperature time series of the Baffin Bay basin obtained from sporadic bottle- and CTD-casts within a 200 m vertical bin (1940–2003; 800–1000 m; 62–80°N; 85–50°W; irregular time intervals; Fig. 7 in Zweng and Münchow, 2006) and a weekly sea surface temperature (SST; 1989-12-31 to 2020-12-31 within a 2 × 2° grid; 67–69°N, 61.5–59.5°W; resolution 1°) time series obtained from the NOAA Optimum Interpolation SST (OISST) dataset (V2; https://psl.noaa.gov/data/gridded/data.noaa.oisst.v2.html; Reynolds et al., 2002) to achieve a longer, more complete history of environmental conditions. Though we recognise the caveat of comparing to surface, satellite derived, temperatures, it is important to note the lack of high resolution, continuous, deep-water temperature data as a more suitable comparison.

Proximal dissolved barium concentrations ($[Ba]_{SW}$) data were compiled from GEOTRACES (GEOTRACES Intermediate Data Product Group, 2021) to investigate the relationship with *Keratoisis* sp. Ba/Ca values and calculate the partition coefficient, D_{Ba}. Analogous to Kershaw et al. (2023), we identified the geographically closest $[Ba]_{SW}$ profile (66.858°N; 59.074°W; 2015-08-03; Thomas et al., 2021) and a representative (matched the sample depth of each *Keratoisis* sp. colony) $[Ba]_{SW}$ value was calculated (linear interpolation between the nearest two measurement depths; 813 m and 1011 m). Data reported in units of nM, assuming atmospheric pressure and ambient room temperature, were converted to nmol.kg^{-1} using a seawater density of 1.025 kg.m^{-3}. $[Ba]_{SW}$ measurements in the modern ocean remain sparse, especially in the Eastern Canadian Arctic, yet the distance between sampling station and the $[Ba]_{SW}$ profile was <130 km (colony-specific distances, depths and interpolated $[Ba]_{SW}$ values reported in supplementary data tables S2). Uncertainty on interpolated $[Ba]_{SW}$ values was estimated using the variability in depth-matched values from the three most proximal profiles to the coral sampling location in Baffin Bay (± 2 SD; 4.35 nmol.kg^{-1}, Thomas et al., 2021). $[Ba]_{SW}$ was converted to seawater Ba/Ca ratios (μmol.mol^{-1}) using a $[Ca]_{SW}$ value of 10.3 mmol.kg^{-1} (Nozaki, 1997). Seawater [Ca] was assigned an error of ±5% to account for variations in salinity. Calculated barium partition coefficients were compared to a previous study by LaVigne et al. (2011) to cross-reference values with other Octocorals.

2.4. Analytical procedures

2.4.1. Sample preparation

Guided by microCT scans (see electronic supplementary material Methods S1, Fig. S3), each sample of *Keratoisis* sp. was sectioned (20–30 mm thickness, perpendicular to main axis) across three separate internodes, embedded in epoxy resin, hand polished (1200 to 4000 grit) and then polished using a petrological polishing machine (6 polishing cycles over 280 min, starting at 9 μm particulate down to 0.3 μm). To achieve an analytical grade polish, sections were processed for a further 20 min at 0.1 μm and visually quality checked under a digital microscope (AmScope) (see supplementary material Fig. S4).

2.4.2. Laser ablation Triple Quadrupole ICP-MS

Keratoisis sp. sections were analysed using an Agilent (Agilent Technologies Inc., CA, USA) 8900 Triple Quadrupole ICP mass spectrometer coupled to an Elemental Scientific Lasers (Bozeman, MT, USA) NWR193 excimer laser ablation system with a TwoVol2 ablation chamber, housed in the Geochemistry laboratory at the University of Southampton. The isotopes ^{7}Li, ^{25}Mg, ^{43}Ca, ^{86}Sr ^{137}Ba and ^{238}U were selected for analysis to investigate the applicability of commonly used geochemistry temperature proxies (Thresher et al., 2010; Lopez Correa et al., 2011; Flöter, 2019; Flöter et al., 2019) and the seawater barium proxy (LaVigne et al., 2011; Thresher et al., 2016; Flöter et al., 2019; Geyman et al., 2019). Samples and standards were ablated using line rasters, where standard analyses consisted of ca. 230 integration cycles of 0.52 s (1.2 mm lines). For sample analysis, five adjacent 50 μm wide transects were ablated on 12 *Keratoisis* sp. sections (four colonies with three internodes each), where each transect consisted of ca. 240–638 integration cycles of 0.52 s (min 1.2 mm; max 3.2 mm). Prior to data collection, samples and standards were ablated to remove any surface contamination (laser power density of 0.6 J cm^{-2}, repetition rate of 40 Hz, and tracking speed of 400 μm.s^{-1}). Typical operating conditions during data collection are fully outlined in Table S3. An on-peak gas

Table 1
Geographic coordinates and depths of the coral colonies analysed in this study alongside hydrographic data, carbonate system parameters, estimated age (yr) and uncertainty. Temperature (T), salinity (S) and dissolved oxygen (O_2) from conductivity-temperature-depth (CTD) casts taken nearby the coral sample sites are provided (Amundsen Science Data Collection, 2021). For ageing estimation and uncertainty methodology, refer to Section 3.5.1.

SITE	LAT.	LONG.	DEPTH (M)	ID	TAXON.	SEAWATER PARAMETERS			ESTIMATED AGE (YR)	AGE UNCERTAINTY (RANGE, YEARS)
						T (°C)	Salinity	O_2 (μmol/kg)		
EASTERN CANADIAN ARCTIC										
DISKO FAN (CANADA)	67.96629	−59.49069	885	23–1	*Keratoisis* sp.	1.12	33.47	200.1	27	9–31
DISKO FAN (CANADA)	67.96631	−59.4899	883	23–6	*Keratoisis* sp.	1.12	33.47	200.1	56	20–64
DISKO FAN (CANADA)	67.96631	−59.48892	879.9	23–10	*Keratoisis* sp.	1.12	33.47	200.1	28	10–32
DISKO FAN (CANADA)	67.9663	−59.48768	876.2	23–16	*Keratoisis* sp.	1.12	33.47	200.1	22	8–25

blank subtraction was performed to the raw counts using the mean of bracketing gas blank analyses. Blank bracketing cut-offs were calculated as the first 30 s and final 45 s of the ablation run. Due to the irregular curvature of the outer surface of the coral, it was necessary to calculate cut-offs using a 4-step rolling difference, where the maximum positive and negative change in ^{43}Ca across the 4-step are indicative of where the resin-coral boundaries are located. Element/Ca ratios were corrected for instrumental drift and mass bias by standard-sample bracketing with glass reference material NIST SRM612 using the values published by Jochum et al. (2011). In addition, a pressed pellet of *Porites* sp. coral JCp-1 (Hathorne et al., 2013) was analysed as an internal consistency standard. For data processing and outlier rejection, we followed Standish et al. (2019). Briefly, outliers defined as ±3 times the interquartile range of raw counts (within the blanks and analysis brackets) were removed from each set of the standards to eliminate anomalous values. External reproducibility of the consistency standards (2σ, n = 14 per standard) are shown in Table 2. Element ratios of the *Keratoisis* sp. sections were secondary normalised to JCp-1 (see Table 2).

2.4.3. Elemental mapping

Outliers were removed from each laser line for elements of the *Keratoisis* sp. sections using a standard deviation (SD) rejection and the data were smoothed using a 5-point moving average. Selection of the number of SD for rejection was dependent on an initial examination of the data patterns and the degree of coherence of the variability observed for each element (see supplementary material Table S4). For each section, five separate smoothed laser lines were mapped onto an equal spaced grid using their X and Y spatial coordinates from the laser ablation system. The dimensions of the grid were governed by the resolution of the data, laser tracking speed (10 μm.s^{-1}) and integration time (0.472 s) and were constructed using the "raster" function of the terra package (Hijmans, 2022) in R (R Core Team, 2022), achieving a resolution of 5 × 50 μm. pixel^{-1} map. To align the elemental maps onto the coral sections, cleaned coral skeletons were carbon coated and mounted to conductive carbon tape and imaged with a Leo 1450VP (Carl Zeiss) variable pressure scanning electron microscope housed within the School of Ocean and Earth Science, University of Southampton.

2.5. Paleo-environmental reconstructions

2.5.1. Age model

Coral elemental ratios need to be translated from distance to age to directly compare to the observational temperature and $[Ba]_{SW}$ record. As radiocarbon data are not available to obtain a specimen-specific age model to complete a timeseries analysis of our geochemical mapping data, instead we derive a genus-specific model based on data derived from the primary literature and calculate the growth rate uncertainty as per Flöter et al. (2019). To achieve this we compiled published linear radial growth rates for *Keratoisis* sp. (n = 13, see supplementary material Table S5) from the returns of a Thomson Reuters Web of Science collection (http://www.webofknowledge.com, accessed 2022-09-30) 'Advanced Search' across all databases with the search term "(*Keratoisis* AND '*growth rate*')"" in the titles, key words and abstracts of all document types, in all languages, for the publication years 1950 to 2021. We also extracted associated environmental metadata (latitude, longitude, water depth, temperature), information on the methodology used, and details about timing (year) and ecoregion (following accepted biogeographical typologies; Bailey, 1998; Spalding et al., 2007), reducing the number of records to 11 publications. Although more complex nonlinear growth modes have been proposed for bamboo corals (e.g., Frenkel et al., 2017) to allow for ontogenetic changes in growth rates (Farmer et al., 2015b), we prefer to opt for a linear model given the limited available chronological data. Non-linearity in growth could be identified by counting periodic bands (Thresher et al., 2004; Roark et al., 2005), however, banding was irregular and frequently ambiguous in the colonies presented in this study (μCTscan, digital microscope images, see supplementary material Fig. S4; SEM images, supplementary material Fig. S5). An absolute (calendar) age model was established for these colonies using the collection year (2021), estimated median growth rate (51 μm.yr^{-1}), and upper and lower quartiles (31 μm.yr^{-1}; 59 μm.yr^{-1}) across all colonies from the literature (n = 21, see supplementary material Table S6). To estimate the relative dating precision for a given sampling point, we started with the sampling year (2021) and integrated one-sided dating uncertainty in years, calculated as follows:

$$\Delta t_{+;-} = \left|\left(\frac{d}{GR_m} + A_{abs}\right) - \left(\frac{d}{GR_{+;-}} + A_{abs}\right)\right| \quad (1)$$

where d is the distance from the outer rim in μm, GR_m is the mean growth rate in μm.yr^{-1}, $GR_{+;-}$ are the respective upper and lower growth rate quartiles in μm.yr^{-1}, and A_{abs} is the year of sampling. Maximum uncertainty values alongside estimated ages for each colony are presented in Table 1.

2.5.2. Intra-individual covariance and reproducibility

Covariance between raw Element/Calcium ratio (hereafter, E/Ca) signals were first compared between each internode of the same colony using the '*ggpairs*' R function of the *GGally* package (v2.1.2; Schloerke et al., 2021). Intra-individual reproducibility in E/Ca signals was analysed using a stratigraphic correlation technique. To accomplish this, the five ablation tracks per internode were first averaged into one transect along the growth axis. Anchor points were assigned by correlating unique peaks and troughs present across the transects of the basal and other two internodes in that colony using the "QAnalySeries" software (v 1.5.1, Kotov and Pälike, 2018). Barium profiles were selected as the basis for assigning anchor points due to the similarity in trends between internodes, allowing for precise alignment of different tracks (Sinclair et al., 2011). The age model established by stratigraphic tuning of Ba/Ca signals was then applied to each of the remaining 5 ratios (Li/Ca, Li/Mg, Mg/Ca, Sr/Ca and U/Ca) to obtain tuned element tracks in each internode (linearly interpolated back to 50 μm intervals) and intra-specific Pearson's correlation scores.

2.5.3. Multi-element, multi-species paleothermometry calibrations

In conjunction with Section 3.5.1, we evaluated the systematics of the Li/Mg, Mg/Ca, Sr/Ca, Ba/Ca, U/Ca and Sr—U multispecies palaeothermometry in published literature for coral and coralline algae. This was achieved using reported values of the five element ratios (standard corrected) in the returns (n = 193, see supplementary material Table S7) of an 'Advanced search' of the Thomson Reuters Web of Science collection (http://www.webofknowledge.com, accessed 2022-09-30) across all databases for "((Li/Mg OR Mg/Ca OR Sr/Ca OR Ba/Ca OR U/Ca OR Sr-U) AND (coral OR coralline algae) AND (temperature OR

Table 2
Selected average JCp-1 elemental ratios normalised to NIST612 as determined over two sessions in May 2022.

Elemental ratio	Mean (n = 13)	2 s.d.	2 s.d. (%)	Difference from reference (%)*
Li/Ca (μmol/mol)	6.73	0.50	7.37	8.77[a]
Mg/Ca (mmol/mol)	4.36	0.18	4.04	3.76[a]
Sr/Ca (mmol/mol)	8.43	0.17	2.00	−4.64[a]
Ba/Ca (μmol/mol)	5.36	0.58	10.90	−28.27[a]
U/Ca (μmol/mol)	1.09	0.03	3.12	−8.67[a]

Isotopes measured: ^{7}Li, ^{26}Mg, ^{43}Ca, ^{88}Sr, ^{138}Ba, ^{238}U.

* Refers to the deviation in mean element ratios relative to GeoRem preferred compositions.

[a] Hathorne et al., 2013.

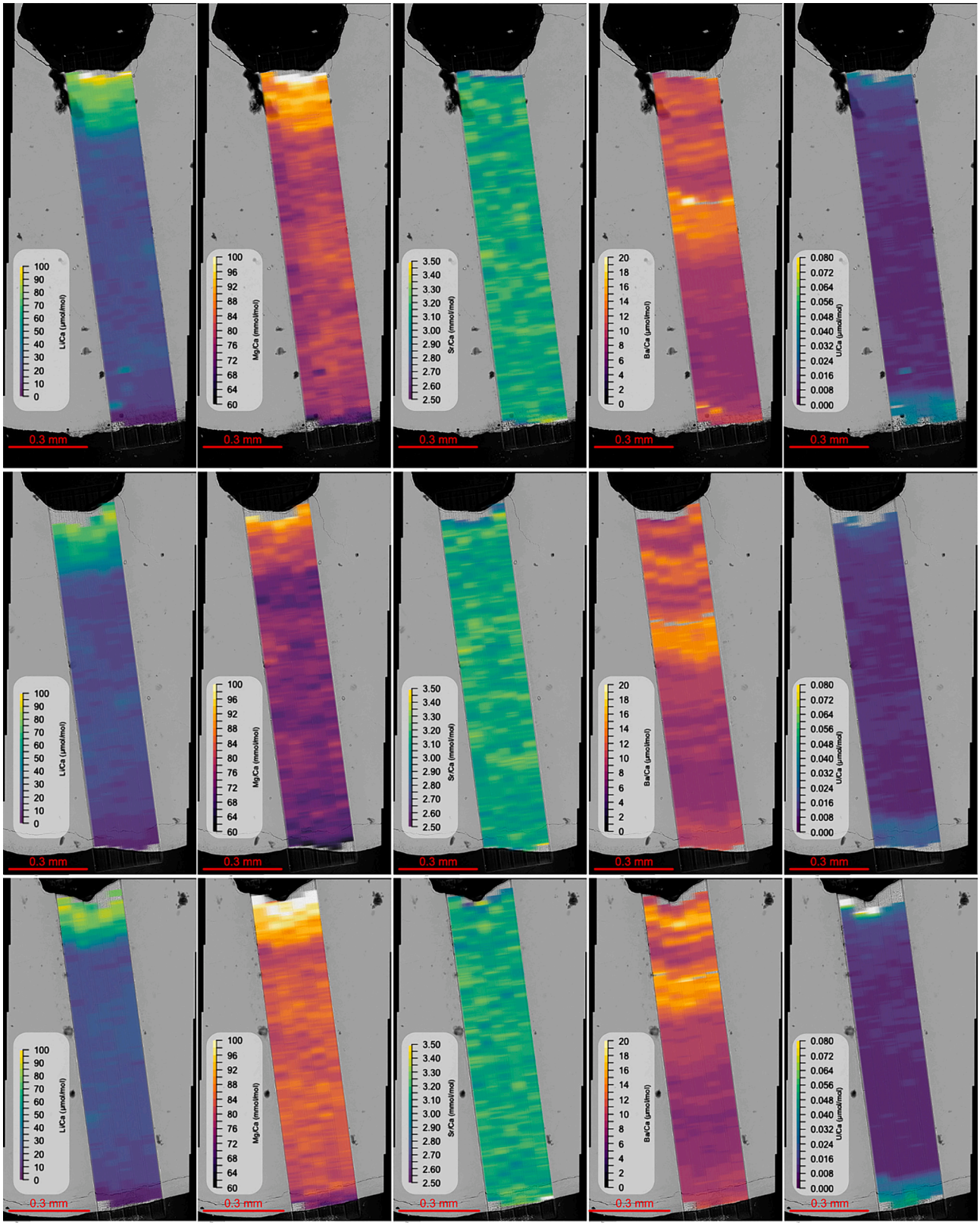

Fig. 1. Two dimensional patterns in *Keratoisis* sp. element ratios (left to right: Li/Ca, Mg/Ca, Sr/Ca, Ba/Ca and U/Ca) analysed by laser ablation and overlain onto a post-ablation SEM image of the basal internode (top row), second internode (middle row) and third internode (bottom row) of colony (*a*) #23–1, (*b*) #23–6, (*c*) #23–10 and (*d*) #23–16. Ratios that clearly match structure elements of the coral include high Li/Ca, Mg/Ca and U/Ca values confined to central axis and low Li/Ca, Mg/Ca values confined to coral wall. Banding is clear in the Barium profiles. Length scales provided in SEM images with colour scales consistent across all colonies provided in panel (e).

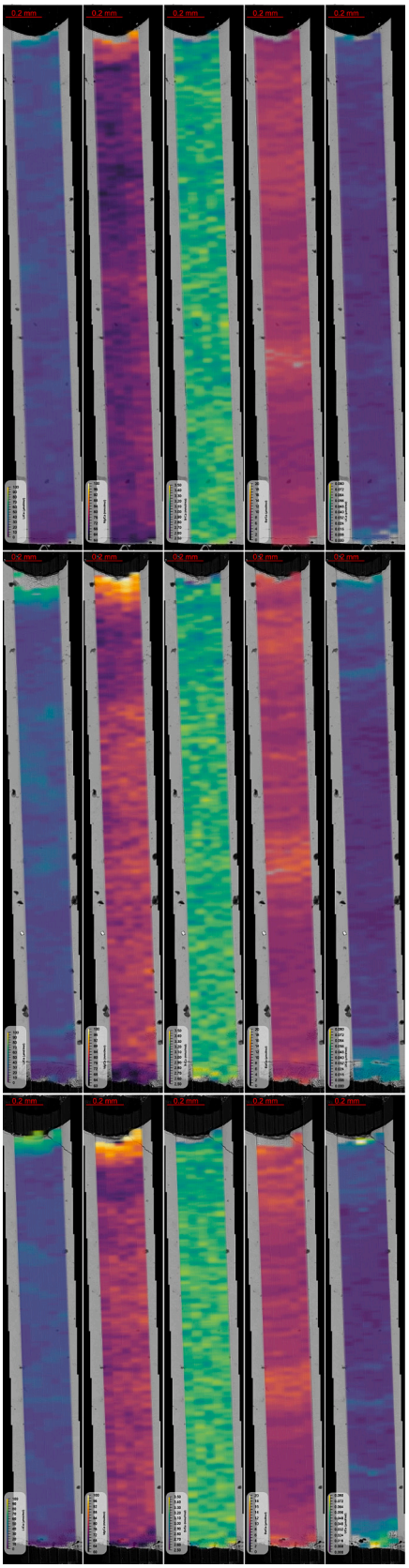

Fig. 1. (*continued*).

thermometry OR thermometer) AND (calibration)") in the titles, key words and abstracts of all document types, in all languages, for the publication years 1950 to 2021. We also extracted associated environmental metadata (latitude, longitude, water depth, temperature), information on the analytical methodology used, type of marine calcifier, mineralogy, details about timing and ecoregion (following

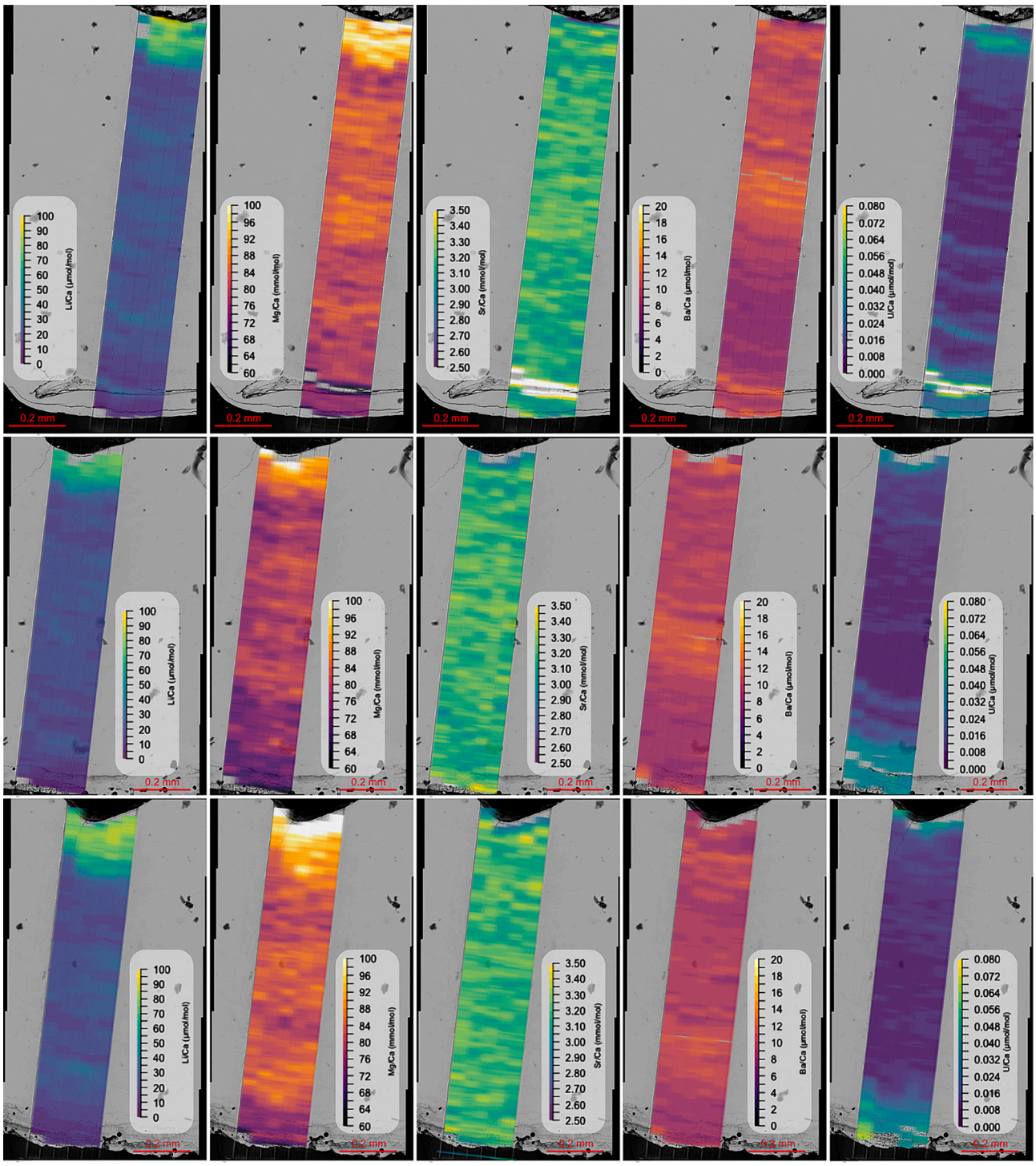

Fig. 1. (*continued*).

accepted biogeographical typologies; Bailey, 1998; Spalding et al., 2007). We include culture experiments in our compilation, incorporating data where seawater carbonate chemistry has not been manipulated. Where data was compiled from other sources, we extracted data from the original publication. Data that was only presented graphically (with decipherable individual data points) were extracted using *WebPlotDigitiser* (v4.6; Rohatgi, 2022). Papers that focused solely on reconstructing temperature from derived empirical calibrations without supporting in-situ instrument measurements (either used to directly compare against element signals or to correlate against satellite derived temperature) were excluded from data extraction, leaving 2637 unique data points across 56 papers (see electronic supplementary material, Data records S1). Alongside data from Kershaw et al. (2023), reported values of seawater barium ($[Ba]_{SW}$) were also compiled from the returns of our literature search, in addition to associated metadata (latitude, longitude, water depth, temperature, salinity, pH), type of marine calcifier and mineralogy ($n = 329$ unique data points across 8 papers; see electronic supplementary material, Data records S1). Published element ratio-temperature (E/Ca-T) and $[Ba/Ca]_{coral}$-$[Ba]_{SW}$ calibration equations were compiled and compared with our own calibrations that evaluate the influence of mineralogy and taxa.

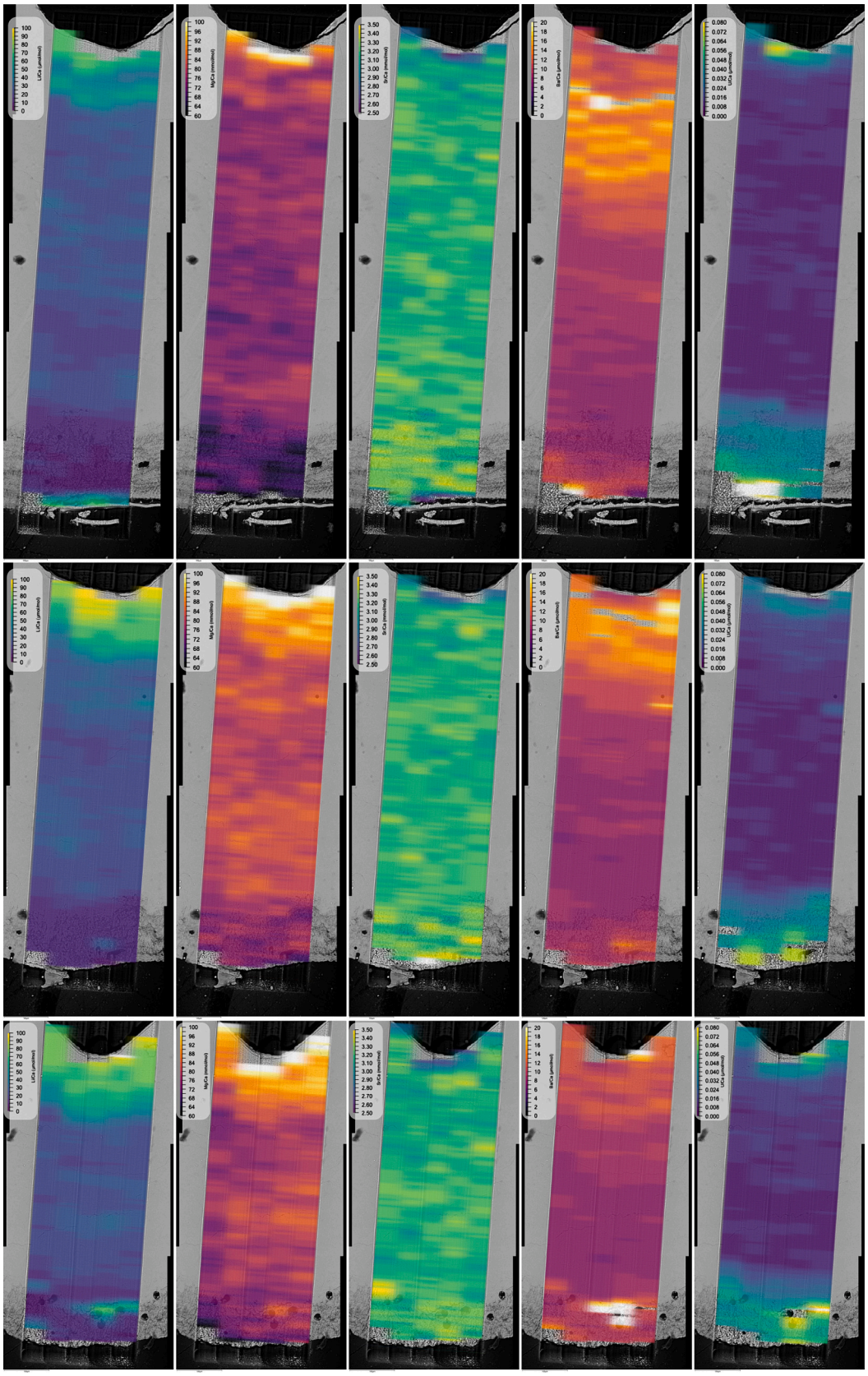

Fig. 1. (*continued*).

2.5.4. Inter-individual reproducibility in reconstructed environmental conditions

Stratigraphically tuned E/Ca determinations in the distance domain (i.e., μm from coral wall) were converted to the time domain using the age model. Reconstructions of temperature and $[Ba]_{SW}$ from *Keratoisis* sp. records was carried out using the derived calibration equations

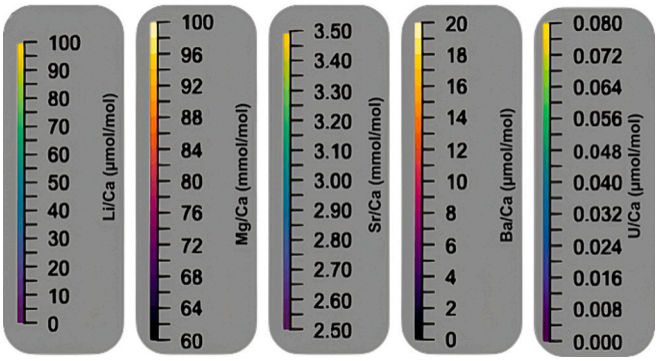

Fig. 1. (*continued*).

(Section 3.5.3) for multispecies high-Mg corals and compared across internodes and between colonies. Reconstructions were linearly interpolated from 10 points a year to 4 points a year (seasonal) and 1 point a year (annual) using the *spline* function from the stats R package (R Core Team, 2022). Mean $[Ba]_{SW}$, mean temperature, and temperature trend (°C. yr^{-1}) were calculated over the shared time period among all colonies, with the latter subsequently compared to trends in SST and deep-water temperature obtained during Section 3.3.

When conducting element analysis for paleoceanographic reconstructions, it is crucial to account for coral skeletal heterogeneities and potential contamination sources. Differences in E/Ca behaviour between outer and central bands suggest distinct mechanisms controlling element uptake in these regions, including but not limited to, skeletal heterogeneity, diagenesis, heat stress, contamination from organic materials, and non-linear growth rates (Adkins et al., 2003; Anagnostou et al., 2011; Gagnon et al., 2007; Stewart et al., 2016; Clarke et al., 2019; Cuny-Guirriec et al., 2019; Lazareth et al., 2016; Thresher and Neil, 2016; Flöter, 2019; Flöter et al., 2019, 2022). While the absence of calcification centres (COCs) and amorphous carbonate infilling in bamboo corals distinguishes them from other coral groups (Noé and Dullo, 2006; Thresher et al., 2004; Andrews et al., 2009; Thresher et al., 2010; Farmer et al., 2015b), reduced and elevated E/Ca values near the central axis and coral wall are still observable in *Keratoisis* spp. (Fig. 1; Flöter et al., 2019). Hence, these sections were removed prior to temperature reconstruction. Despite these exclusions, the majority of the coral internode sections (mean: 85.9%, range: 73.7–95.5%) were considered for paleotemperature reconstruction.

2.6. Statistical analyses

Tests for intra-individual covariance among *Keratoisis* sp. elements ($n = 7$) were carried out using Spearman's rank (monotonic) correlations. To establish an empirical relationship between coral E/Ca and in-situ environmental conditions (Section 3.5.3), and reconstructed temperature vs time calculations (Section 3.5.4), we used an ordinary least squares (OLS) regression technique (type I; Alibert and McCulloch, 1997; Quinn and Sampson, 2002) and compared with a reduced major axis (RMA) regression model (type II; Cobb, 1998), with temperature as the independent variable and coral element/Ca as the dependent variable. The OLS technique assumes error only in the measurement of the dependent variable, whilst a RMA assumes error in the measurement of both the dependent and independent variables and is more suitable for use with geologic data. The slope of the equation produced by the RMA regression is equal to the slope of the equation of the OLS regression divided by the correlation coefficient (e.g., Cobb, 1998).

To test the individual and interactive effects of between-individual (colony) and within-individual (internode) variation on: (i) the mean reconstructed temperature (intercept) and trend (slope) calculated using the element paleothermometry proxy, and (ii) the mean reconstructed $[Ba]_{SW}$ calculating using the Ba/Ca-$[Ba]_{SW}$ proxy, repeated measures two-factor analysis of variance models (ANOVAs) were created. As internodes were sampled repeatedly (to achieve different interpolations), we accounted for pseudoreplication by incorporating interpolation as a random factor (random intercepts) in linear mixed effect (LME) models (Zuur et al., 2009). We assessed model assumptions by visual inspection of standardised residuals vs fitted values plots, Q-Q plots, and Cook's distance (Zuur et al., 2010). When homogeneity of variance was violated, we utilised a *varIdent* variance-covariance structure and generalised least-squares (GLS) estimation (Pinheiro et al., 2022; Pinheiro and Bates, 2000; West et al., 2014), which allows residual spread to differ between the individual explanatory variables. We determined the optimal fixed-effects structure using backward selection informed by Akaike Information Criteria (AIC) and inspection of model residual patterns. For the GLS analysis, we determined the optimal variance-covariance structure through restricted maximum-likelihood (REML) estimation by comparing the initial ANOVA model without variance structure to equivalent GLS models incorporating specific variance terms. The suitability of these models was compared against the initial ANOVA model using the AIC and by visualising model residuals. Finally, we determined the optimal fixed structure of the most suitable model through backward selection using the likelihood ratio test with maximum-likelihood (ML) estimation (West et al., 2014; Zuur et al., 2010).

All data processing was carried out in R (v4.2.2, R Core Team, 2022) using the *GGally* (Schloerke et al., 2021), *lmodel2* (Legendre, 2018), *nlme* (Pinheiro et al., 2022; Pinheiro and Bates, 2000), *patchwork* (Pedersen, 2022), *stats* (R Core Team, 2022), *terra* (Hijmans, 2022) *tidyverse* (Wickham et al., 2019) and *viridis* packages (Garnier et al., 2021). All code associated with this study has been deposited on Github (tjwbenth/BambooCoral-LAICPMS) and a summary of statistical models is included in the supplementary material (Models S1-S3).

3. Results

3.1. Patterns in coral elements

The co-located 2D maps of skeletal element composition exhibit coherent lateral variability across each colony's internode, as geochemical patterns are aligned to the same coral section and observable in all specimens, suggesting that these patterns are representative of *Keratoisis* sp. (Fig. 1). The following patterns are typically evident in each image: elevated Li/Ca, Mg/Ca, U/Ca and depleted Sr/Ca are observable near the central axis, with depleted Li/Ca, Mg/Ca, Sr/Ca and elevated U/Ca found near the coral wall. Examination of SEM and digital microscope images reveal a less dense calcite at the coral radial wall, which suffered acute cracking during the ablation (supplementary material Fig. S5) and a denser band of calcite that encompasses the hollow central axis (supplementary material Fig. S4). The Sr/Ca images demonstrate significant heterogeneity in both dimensions, with elevated values near minute stress fractures along the laser tracks, indicating that

this element ratio does not follow a clear structure over time. Radial banding in Ba/Ca is visible across all colonies, with each band of elevated concentrations reproduced further from the coral wall from the basal internode upward, suggesting these are representing repeating events experienced by every internode calcifying at the time. Outside of the elevated values at the outer edge of the coral, U/Ca ratios are more or less constant throughout the internode with some banding visible in the larger colonies.

3.1.1. *Intra-individual E/Ca variability and reproducibility*

Frequency distributions of skeletal elements in *Keratoisis* sp. from Baffin Bay (Fig. 2) reveal that all elements, with the exception of Mg/Ca, exhibit overlapping distributions between internodes. Three of the four colonies exhibited the greatest variance in element ratios in the basal internode. Overall, we find a reproducible positive covariance between Mg/Ca and Li/Ca within all colonies ($p < 0.001$), with positive monotonic correlation scores (range, 0.226–0.857 in Spearman's rank). Generally, Sr/Ca and U/Ca exhibit a weak negative covariance (Spearman's rank, range: −0.084 to −0.281, $p < 0.001$). However, a positive

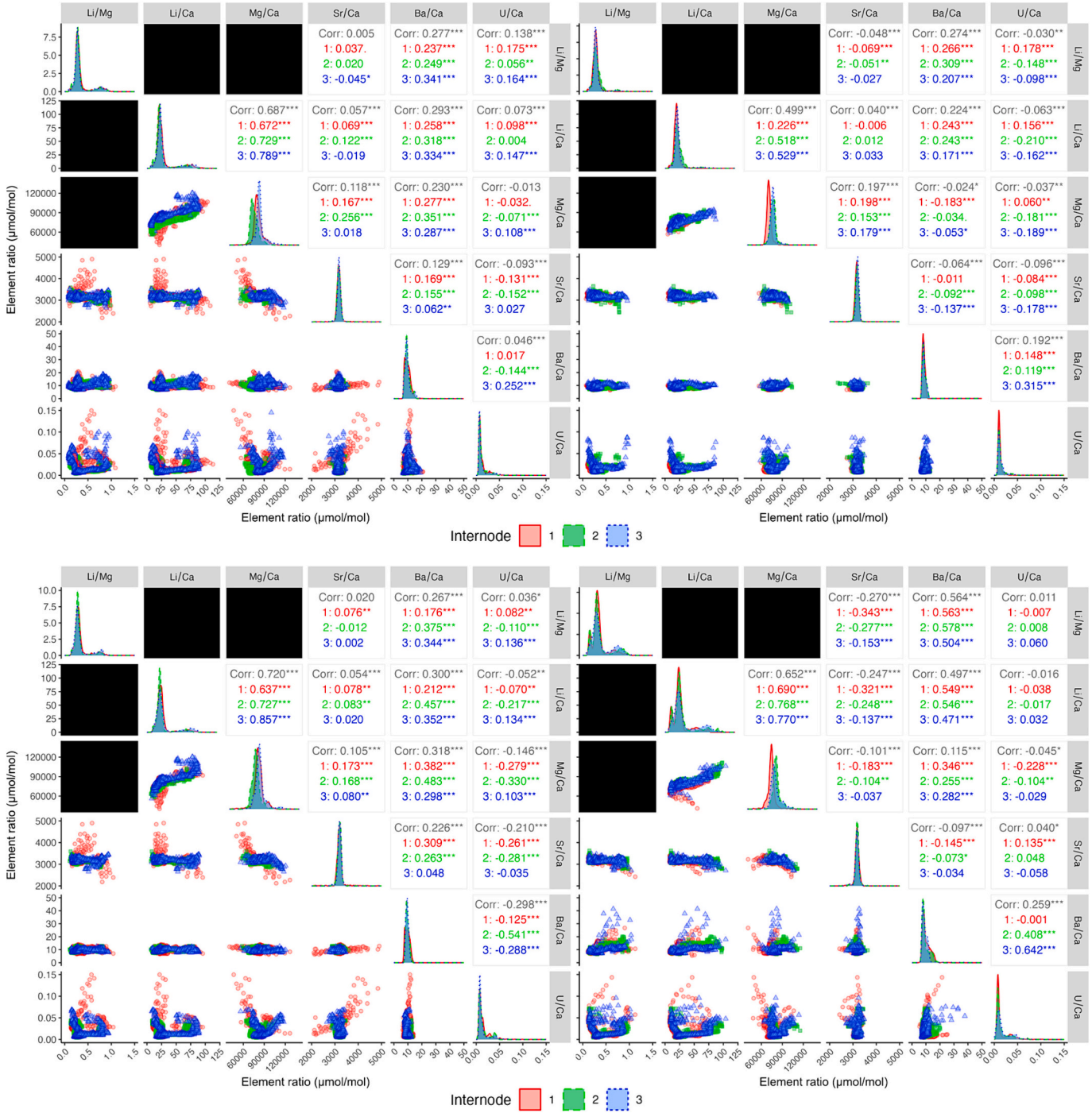

Fig. 2. Covariance (Spearman's Rank; top right subplots) and distribution (bottom left subplots) of Li/Mg, Li/Ca, Mg/Ca, Sr/Ca, Ba/Ca and U/Ca ratios (μmol/mol) within the basal internode (**red**), second internode (**green**) third internode (**blue**) and combination of all internodes (**grey**) of *Keratoisis* sp. colonies (*a*) #23–1 (left) and #23–6 (right), and (*b*) #23–10 (left) and #23–16 (right). Significance of Spearman's rank: *, p < 0.05; **, p < 0.01; ***, p < 0.001. (For interpretation of the references to colour in this figure legend, the reader is referred to the web version of this article.)

covariance is present in the first internode in one colony (Fig. 2b, colony #23–16; Spearman's rank, 0.135, $p < 0.001$) but not evident in the third internode of the three colonies (Fig. 2a, colony #23–6; 2b, colony #23–10, #23–16). Ba/Ca exhibits a consistent positive co-variance within all colonies and between individual internodes with Li/Mg ($p < 0.001$; Spearman's rank 0.176–0.578) and Li/Ca ($p < 0.001$, Spearman's rank 0.171–0.549) but not Mg/Ca (colony #23–6: $p < 0.001$, Spearman's rank −0.183; colony #23–1, #23–10 and #23–16: $p < 0.001$, Spearman's rank 0.255–0.483), Sr/Ca or U/Ca.

3.1.2. Inter-individual E/Ca variability and reproducibility

When the entire history of the coral is evaluated without rejection of the inner and outer walls, we find a decrease in values with increasing distance from the central axis across all specimens and their internodes for Li/Ca and Mg/Ca (Li/Ca: OLS slope range − 0.46 to −0.81, R^2 range, 0.21–0.68, all $p < 0.001$; Mg/Ca: OLS slope range − 0.2 to −0.81, R^2 range, 0.04–0.66, all $p < 0.001$; Table 3; Fig. 3), with both ratios exhibiting respectively large ranges (Li/Ca: 4.54–113.23 μmol.mol^{-1}; Mg/Ca: 41.03–126.69 mmol.mol^{-1}) but different coefficients of variation (Li/Ca: 9–19%; Mg/Ca: 2–4%). In colony #23–6, mean (± 2 s.d.) Mg/Ca in the basal internode is lower (71.27 ± 4.25 mmol.mol^{-1}) than the other replicates (#23–1: 80.42 ± 5.41 mmol.mol^{-1}; #23–10: 81.90 ± 5.14 mmol.mol^{-1}; #23–16: 74.31 ± 4.82 mmol.mol^{-1}), with weaker trends across each internode (OLS slope range, −0.2 to −0.35) and a poor level of explained variance (R^2 range, 0.04–0.12). We found low coefficients of variation in Sr/Ca values across all colonies and a positive trend (increasing values with distance from central axis; $p < 0.01$ - <0.001; Table 3), albeit with a lower amount of variance explained (median R^2: 0.15) relative to that observed for Li/Ca and Mg/Ca (Li/Ca: median R^2, 0.51; Mg/Ca: median R^2, 0.53). For U/Ca, we observed positive trends in two out of the four colonies, with the strongest trends within the first two internodes (OLS slope range: 0.25 to 0.41, $p < 0.001$; R^2 range, < 0.01–0.17) albeit with high coefficients of variation (13–21%; Table 3). Excluding the inner and outer edges of the internodes results in a general reduction in the OLS slope and a reduced amount of variance explained for the Li/Ca and Mg/Ca trends, mixed changes for trends of Sr/Ca, and a higher OLS slope, and greater variance explained, for U/Ca trends across all specimens (Table 3). The coefficients of variation for Li/Ca, Mg/Ca and Sr/Ca demonstrated no improvement after these exclusions, and in some U/Ca trends worsened (colony #23–1, #23–16 and #23–6).

With the exception of Sr/Ca, stratigraphic tuning using the Ba/Ca-based age model revealed strong synchronicity in element signals between the basal and adjacent internodes of *Keratoisis* sp. (mean correlation score ± s.d.; 0.838 ± 0.132, $n = 12$; Fig. 3). However, the magnitude of synchronicity widely differed between the colonies and element signals were generally synchronised better between the basal and second internode than the basal and third internode (Table 4). Specifically, element signal pattern synchronicity (mean correlation score ± s.d, n = 12) was greatest in U/Ca (0.747 ± 0.115) and worst in Sr/Ca (0.147 ± 0.227), with Li/Ca, Mg/Ca and Li/Mg all exhibiting similar correlation strengths (0.602 ± 0.317, 0.569 ± 0.294 and 0.530 ± 0.357, respectively).

3.2. Multi-element, multi-species paleo-environment calibrations

From our global-scale analysis of the compiled literature (see electronic supplementary material Dataset S1), we find significant linear temperature dependency in aragonitic, high-Mg calcite and Octocoral Mg/Ca, U/Ca and Ba/Ca (Fig. 4; Table 5a: $p = 0.001$), while Li/Mg demonstrates an exponential relationship with temperature in both aragonitic and all high-Mg calcitic taxa (Octocorals and coralline algae) and a linear relationship in Octocorals (Fig. 4a; Table 5b). The gradient and intercept values in the ordinary least squares (OLS) and reduced major axis (RMA) regressions exhibit a high degree of similarity (± 2 s.d.) in all paleo-environment calibrations (Table 5). As such, consistent with previous studies, we present OLS regression calibrations, but it is important to note that we find, in practice, that outcomes are not dependent on regression method. Due to the inherent limitations of nonlinear models, where the coefficient of determination is an inadequate measure for the goodness of fit (Spiess and Neumeyer, 2010), we encountered difficulties in determining the variance explained by temperature for aragonitic and high-Mg calcitic Li/Mg. Nevertheless, our calibration coefficients for the Li/Mg proxy based on both high-Mg calcitic and aragonitic corals align with values presented in previous studies (Table 5b; Montagna et al., 2014; Stewart et al., 2020), providing consistency in our findings. Ranking global-scale Octocoral E/Ca temperature relationships variance explained (R^2) alongside proxy sensitivity (element unit change per °C) from highest to lowest gives an order of Mg/Ca > U/Ca > Ba/Ca > Li/Mg > Sr/U > Sr/Ca (Table 5a), indicating that Mg/Ca and U/Ca appear to have strong potential for paleothermometry in high-Mg calcitic Octocorals.

The barium partition coefficient ($D_{Ba} = Ba/Ca_{coral}/Ba_{SW}$) is negatively correlated with temperature in aragonitic corals with evidence of a linear correlation in high-Mg calcitic Stylasteridae (Kershaw and et al., 2023), though uncertainty (± 2 s.d.) is high for both the intercept (± 19.9, OLS regression) and gradient (± 13.9, OLS regression). We were unable to determine the relationship between D_{Ba} and temperature in Octocorals due to a lack of accompanying in-situ environmental data from the literature, however, D_{Ba} varied across the four *Keratoisis* colonies examined here (± 0.1 within colonies, ± 0.4 across colonies; Fig. 4b) with between colony variation greater than the analytical uncertainty (± 0.12; Fig. 4b). $[Ba]_{SW}$–Ba/Ca demonstrates a linear relationship across all taxa and mineralogies (Table 5a; Fig. 4b) with the steepest $[Ba]_{SW}$-Ba/Ca regression (forced through a zero-intercept) exhibited in high-Mg Stylasteridae (*Errina* sp., *Errinopsis* sp., *Cheiloporidion* sp.; $[Ba]_{SW} = 7.260$ (± 0.169)*Ba/Ca, $R^2 = 0.99$). Although we display data from mixed mineralogy corals, they were not used in any of the regression analyses and, for simplicity, we only compare to peer-reviewed published equations with the highest degree of variance explained ($R^2 > 0.6$, Table 5; complete listing in supplementary material, Table S8). In brief, our compilation of existing global literature revealed no previous Sr/U, U/Ca, Ba/Ca and D_{Ba} temperature calibrations for high-Mg calcitic corals (Octocorals, Stylasteridae), with only Mg/Ca and Sr/Ca temperature calibrations found for high-Mg coralline algae.

3.3. Paleo-environment reconstruction

3.3.1. Temperature

As Mg/Ca demonstrates consistent intra-individual patterns (Table 4; Fig. 1; Fig. 3) and the strongest correlation and sensitivity to temperature ($r = 0.93$, $p < 0.001$, $R^2 = 0.87$; 0.316 ± 0.026 °C/mmol/mol; Table 5a; Fig. 4), we focus on temperature reconstructed using the *Keratoisis*-specific age model, the Octocoral-derived calibration equation, and the stratigraphically tuned Mg/Ca signals. Overall, the Mg/Ca proxy demonstrates significant seasonal, annual and interannual variation in the mean predicted temperature time series (solid line; Fig. 5a) within all colonies. Mean predicted temperature time series are offset by up to 2 °C within internodes from the same individual and up to 5 °C among individuals (between colonies). However, in colony #23–6 (and, arguably, #23–16 and #23–1) the mean reconstructed temperature time series overlaps the range of in-situ measurements from previous records for deep-water Baffin Bay (0.39 °C to 1.36 °C). There are also synchronised multiannual cycles in reconstructed temperature between 3 out of the 4 colonies' basal internodes (#23–1, #23–10 and #23–16) near the years 2005 and 2013 (yellow arrows; Fig. 5a). Assuming each internode is of equal importance within a colony, leveraging each replicate time series by averaging reduced the uncertainty (95% CI's) of reconstructed temperature from ±4.25 °C (range: 3.99–4.52 °C) to ±1.92 °C (range: 0.02–5.91 °C) when seasonally interpolated and to ±2.20 °C (range: < 0.01–4.63 °C) when annual interpolated.

Table 3
Summary Table of mean element ratios (± 2 standard deviations) measured in each full internode or with both the outer and inner edges excluded (central section, temperature proxies only) across all *Keratoisis* sp. colonies. Coefficient of variation (CV) and range of values are also presented. Significance of OLS regression: *, $p < 0.05$; **, $p < 0.01$; ***, $p < 0.001$.

E/Ca	*units*	*Colony ID*	*Internode*	*Section*	*Mean ± 2sd*	*CV*	*Range*	*Slope*	*Significance*	R^2
Li/Ca	μmol/mol	#23–1	1	Full	30.73 ± 6.84	12%	113.23–5.48	**−0.73**	***	**0.54**
				Central	19.52 ± 4.67	12%	44.79–5	**−0.53**	***	**0.28**
			2	Full	27.93 ± 5.02	9%	86.55–6.05	**−0.75**	***	**0.57**
				Central	17.9 ± 3.38	9%	38.71–6.18	**−0.6**	***	**0.36**
			3	Full	30.02 ± 5.15	9%	91.58–5.45	**−0.73**	***	**0.53**
				Central	19.95 ± 3.12	8%	31.43–5.58	**−0.59**	***	**0.35**
		#23–10	1	Full	27.6 ± 7.06	12%	95.60–9.24	**−0.61**	***	**0.37**
				Central	20.79 ± 4.28	10%	32.61–8.42	**−0.3**	***	**0.09**
			2	Full	25.86 ± 5.12	10%	79.59–6.69	**−0.66**	***	**0.44**
				Central	23.27 ± 4.69	10%	72.62–7.86	**−0.64**	***	**0.41**
			3	Full	31.64 ± 7.6	12%	89.48–8.22	**−0.73**	***	**0.53**
				Central	27.71 ± 6.84	12%	81.64–7.49	**−0.7**	***	**0.49**
		#23–16	1	Full	28.01 ± 6.3	11%	76.24–7.68	**−0.63**	***	**0.4**
				Central	20.05 ± 4.46	11%	62.94–7.01	**−0.55**	***	**0.3**
			2	Full	31.77 ± 7.77	12%	98.24–9.67	**−0.81**	***	**0.66**
				Central	25.18 ± 6.36	12%	81.68–8.95	**−0.81**	***	**0.65**
			3	Full	35.81 ± 11.07	19%	104.04–9.17	**−0.83**	***	**0.68**
				Central	32.34 ± 10.12	19%	94.92–8.37	**−0.81**	***	**0.65**
		#23–6	1	Full	19.95 ± 4.71	12%	50.24–4.54	**−0.69**	***	**0.48**
				Central	17.49 ± 3.71	11%	31.57–5.54	**−0.74**	***	**0.55**
			2	Full	24.17 ± 5.44	11%	69.54–9.57	**−0.5**	***	**0.25**
				Central	20.59 ± 4.83	11%	39.03–8.73	**−0.47**	***	**0.22**
			3	Full	23.25 ± 5.37	11%	87.07–7.38	**−0.46**	***	**0.21**
				Central	19.13 ± 4.08	11%	32.48–7.66	**−0.4**	***	**0.16**
Mg/Ca	mmol/mol	#23–1	1	Full	80.42 ± 5.41	3%	112.94–56.34	**−0.73**	***	**0.53**
				Central	75.26 ± 4.63	3%	82.78–54.22	**−0.38**	***	**0.15**
			2	Full	74.23 ± 3.69	2%	98.61–56.38	**−0.72**	***	**0.52**
				Central	69.45 ± 3.22	2%	78.41–55.6	**−0.45**	***	**0.21**
			3	Full	84.55 ± 3.7	2%	111.69–69.15	**−0.64**	***	**0.4**
				Central	79.32 ± 3.14	2%	85.14–67.35	**−0.34**	***	**0.11**
		#23–10	1	Full	81.9 ± 5.14	3%	126.69–36.69	**−0.75**	***	**0.56**
				Central	77.42 ± 4.47	3%	86.78–35.31	**−0.61**	***	**0.37**
			2	Full	78.13 ± 5.03	3%	109.32–58.17	**0.75**	***	**0.56**
				Central	75.06 ± 4.82	3%	105.21–55.98	**−0.72**	***	**0.52**
			3	Full	85.47 ± 5.64	3%	120.54–56.14	**−0.69**	***	**0.47**
				Central	80.96 ± 5.34	3%	110.53–54.03	**−0.7**	***	**0.49**
		#23–16	1	Full	74.31 ± 4.82	3%	106.66–41.03	**−0.74**	***	**0.55**
				Central	70.07 ± 3.95	3%	79.52–46.42	**−0.64**	***	**0.41**
			2	Full	82.39 ± 4.99	3%	115.48–66.33	**−0.74**	***	**0.55**
				Central	77.81 ± 4.29	3%	91.62–63.84	**−0.79**	***	**0.63**
			3	Full	81.24 ± 6.94	4%	113.64–56.83	**−0.81**	***	**0.66**
				Central	78.01 ± 6.68	4%	109.36–54.7	**−0.79**	***	**0.63**
		#23–6	1	Full	71.27 ± 4.25	3%	91.30–56.68	**−0.21**	***	**0.04**
				Central	68.07 ± 4	3%	77.68–58.09	**0.33**	***	**0.11**
			2	Full	77.06 ± 4.94	3%	103.91–60.67	**−0.2**	***	**0.04**
				Central	73.68 ± 4.56	3%	83.66–59.96	0.1	*	0.01
			3	Full	76.82 ± 4.38	3%	98.12–58.56	**−0.35**	***	**0.12**
				Central	73.07 ± 3.92	3%	80.95–62.11	0.1	*	0.01
Ba/Ca	μmol/mol	#23–1	1	Full	9.97 ± 1.42	7%	20.76–6.83			
			2	Full	10.01 ± 1.42	7%	16.2–6.56			
			3	Full	10.05 ± 1.36	6%	19.02–6.7			
		#23–10	1	Full	9.68 ± 1.11	6%	14.01–6.33			
			2	Full	9.65 ± 1.1	6%	13.27–7.41			
			3	Full	9.46 ± 1.09	6%	12.46–7.66			
		#23–16	1	Full	10.36 ± 1.8	8%	26.73–5.4			
			2	Full	9.87 ± 1.52	7%	20.16–6.58			
			3	Full	9.74 ± 2.78	11%	41.4–6.84			
		#23–6	1	Full	8.41 ± 0.73	4%	11.3–6.28			
			2	Full	8.78 ± 0.88	5%	13.02–6.51			
			3	Full	8.83 ± 0.95	5%	13.99–6.63			
Sr/Ca	mmol/mol	#23–1	1	Full	3.15 ± 0.11	2%	3.49–2.86	0.14	*	0.02
				Central	3.3 ± 0.1	2%	3.49–2.99	−0.07		<0.01
			2	Full	3.15 ± 0.11	2%	3.54–2.9	−0.04		<0.01
				Central	3.3 ± 0.1	2%	3.53–3.11	**−0.34**	***	**0.12**
			3	Full	3.15 ± 0.11	2%	3.53–2.78	**0.32**	***	**0.1**
				Central	3.31 ± 0.1	1%	3.45–3.12	−0.15	*	0.02
		#23–10	1	Full	3.2 ± 0.17	3%	6.05–2.69	0.17	**	0.03
				Central	3.37 ± 0.17	2%	6.05–3.05	0.19	**	0.03
			2	Full	3.19 ± 0.12	2%	3.57–2.98	**0.28**	***	**0.08**
				Central	3.34 ± 0.12	2%	3.57–2.98	0.06		<0.01
			3	Full	3.18 ± 0.12	2%	3.63–2.9	**0.32**	***	**0.1**
				Central	3.35 ± 0.13	2%	3.63–2.94	0.19	**	0.04

(*continued on next page*)

Table 3 (*continued*)

E/Ca	units	Colony ID	Internode	Section	Mean ± 2sd	CV	Range	Slope	Significance	R^2
		#23–16	1	Full	3.17 ± 0.14	2%	3.58–2.53	**0.45**	***	**0.2**
				Central	3.34 ± 0.13	2%	3.58–2.76	**0.27**	***	**0.08**
			2	Full	3.18 ± 0.12	2%	3.61–2.91	**0.64**	***	**0.41**
				Central	3.34 ± 0.11	2%	3.61–3.17	**0.5**	***	**0.25**
			3	Full	3.17 ± 0.14	2%	3.64–2.83	**0.58**	***	**0.33**
				Central	3.32 ± 0.14	2%	3.64–2.83	**0.57**	***	**0.32**
		#23–6	1	Full	3.16 ± 0.12	2%	3.56–2.86	**0.48**	***	**0.23**
				Central	3.32 ± 0.13	2%	3.56–3.06	**0.37**	***	**0.13**
			2	Full	3.17 ± 0.13	2%	3.81–2.47	**0.52**	***	**0.27**
				Central	3.33 ± 0.12	2%	3.81–3.09	**0.43**	***	**0.18**
			3	Full	3.19 ± 0.11	2%	3.65–3.03	**0.52**	***	**0.27**
				Central	3.35 ± 0.11	2%	3.65–3.14	**0.35**	***	**0.13**
U/Ca	nmol/mol	#23–1	1	Full	11.99 ± 3.93	17%	50.01–4.55	0.08		<0.01
				Central	11.18 ± 3.81	17%	50.01–4.55	**0.48**	***	**0.23**
			2	Full	10.67 ± 3.09	15%	31.49–4.17	0.02		<0.01
				Central	10.62 ± 3.09	15%	31.49–4.17	**0.45**	***	**0.2**
			3	Full	14.53 ± 5.2	16%	157.76–4.48	0.09		<0.01
				Central	10.73 ± 3.29	15%	59.6–4.48	**0.45**	***	**0.2**
		#23–10	1	Full	16.41 ± 7.75	21%	162.79–5.28	**0.25**	***	**0.06**
				Central	15.97 ± 7.96	21%	162.79–5.28	**0.55**	***	**0.3**
			2	Full	15.48 ± 4.68	17%	50.94–4.77	**0.41**	***	**0.17**
				Central	15.99 ± 5.01	17%	50.94–4.77	**0.48**	***	**0.23**
			3	Full	17.18 ± 6.33	18%	74.84–4.79	0.06		<0.01
				Central	16.59 ± 6.88	18%	74.84–4.79	**0.35**	***	**0.13**
		#23–16	1	Full	18 ± 7.93	18%	155.87–4.83	**0.34**	***	**0.11**
				Central	17.09 ± 6.54	16%	155.87–4.83	**0.47**	***	**0.47**
			2	Full	17.9 ± 5.99	18%	77.52–4.96	**0.38**	***	**0.15**
				Central	16.62 ± 6.04	18%	77.52–4.96	**0.57**	***	**0.32**
			3	Full	20.98 ± 9.31	19%	104.33–4.52	0.23	**	0.05
				Central	21.5 ± 9.83	19%	104.33–4.52	0.24	**	0.06
		#23–6	1	Full	11.74 ± 3.27	14%	42.29–6.57	−0.02		<0.01
				Central	12.06 ± 3.16	13%	32.95–6.57	**0.33**	***	**0.11**
			2	Full	14.02 ± 3.59	13%	53.76–6.66	0.06		<0.01
				Central	14.21 ± 3.58	13%	53.76–6.66	**0.36**	***	**0.13**
			3	Full	15.13 ± 5.52	16%	94.79–6.06	0.07		<0.01
				Central	14.74 ± 4.6	15%	82.41–6.06	**0.41**	***	**0.17**

Over the period common to all corals (2003 to 2016), we find that Mg/Ca reconstructed deep-water temperatures exhibited subtle, but significant, cooling trends (Table 6), though the rate of cooling and mean reconstructed temperature differed across colonies and internodes (Fig. 5a). Similar to the multi-taxa calibrations previously demonstrated (Table 5; Fig. 4), the gradients of both OLS and RMA regressions displayed a notable degree of resemblance. The disparities between these two regression methods (± 2 s.d.) lead us to exclusively refer to OLS regressions for consistency. We found strong and marginal random effects of interpolation on the mean temperature between 2003 and 2016 ($T_{[rec]}$ mean; L-ratio = 25.666, d.f. = 1, $p < 0.0001$) and OLS slopes ($T_{[rec]}$ trend; L-ratio = 2.154, d.f. = 1, $p = 0.071$), respectively, and hence, we retained the random effects in both models. Linear mixed models revealed strong dependency of the $T_{[rec]}$ mean and $T_{[rec]}$ trend on the colony × internode interaction ($T_{[rec]}$ mean: L-ratio = 117.338, d.f. = 6, $p < 0.0001$; $T_{[rec]}$ trend: L-ratio = 20.63, d.f. = 6, $p < 0.01$; supplementary material model S1 and S2). Investigating the individual effects demonstrated that colony was more important than internode for the $T_{[rec]}$ trend (Colony: L-ratio = 66.93, d.f. = 9, $p < 0.0001$; Internode: L-ratio = 20.76, d.f. = 8, $p < 0.01$), whilst internode was more important than colony for the $T_{[rec]}$ mean (Colony: L-ratio = 175.82, d.f. = 9, $p < 0.0001$; Internode: L-ratio = 189.08, d.f. = 8, $p < 0.0001$). Mean $T_{[rec]}$ (un-interpolated ± s.e.) across this time period ranged from 4.77 ± 0.03 to 1.04 ± 0.02 °C (Fig. 5a). A stronger cooling $T_{[rec]}$ trend was reconstructed in one colony (23–10; −0.22 ± 0.04 to −0.16 ± 0.03 °C.yr^{-1}) compared to the other three colonies in this study, which all exhibited $T_{[rec]}$ trends similar to Optimum Interpolation SST data (dashed vertical yellow line, Fig. 5a). Mean $T_{[rec]}$ became more uncertain (± s.e.) as the data was interpolated to longer timeframes (un-interpolated: ± 0.021 to 0.155; seasonally interpolated: ± 0.034 to 0.195; annual interpolated: ± 0.093 to 0.374) with an overall weaker cooling $T_{[rec]}$ trend when the data was seasonally interpolated.

3.3.2. $[Ba]_{SW}$

Using the $Ba/Ca_{Octocoral} - [Ba]_{SW}$ calibration (calculated in Section 4.2), we find highly reproducible reconstructions of seawater barium in our *Keratoisis* sp. colonies (Fig. 5b) with mean uncertainty (95% CI's) of ±2.24 nmol.kg^{-1} (range: 1.62–4.94 nmol.kg^{-1}) and strong seasonal and annual variation recorded. A reproducible, multi-year spike in $[Ba]_{SW}$ between 2000 and 2005 can be observed across three colonies (#23–16, #23–10 and #23–1), with evidence of this event occurring ~2 years earlier in the remaining colony, most likely an indication of the uncertainty in our age models. Over the period common to all colonies (1998–2021), mean $[Ba]_{SW}$ was dependent on a colony × internode interaction (L-ratio = 32.23, d.f. = 6, $p < 0.0001$; supplementary material, model S3) but we found no influence of interpolation as a random effect (L-ratio = 0.009, d.f. = 1, $p = 0.461$). Specifically, un-interpolated mean $[Ba]_{SW}$ (± s.e.) ranged from 52.6 ± 0.4–67.7 ± 1.2 nmol.kg^{-1} across the different colonies and is in good agreement with depth-approximated $[Ba]_{SW}$ values from the geographically closest profile (52.4–52.7 nmol.kg^{-1}; Fig. 5b). There is no consistent change in mean $[Ba]_{SW}$ from the basal internode upward, but there is evidence of a decreasing mean $[Ba]_{SW}$ and reduced variability in $[Ba]_{SW}$ when moving from the smallest (#23–16) to largest (#23–6) colony.

4. Discussion

Differences in element behaviour between the outer, inner and central bands of *Keratoisis* sp. internodes strongly suggest different controlling mechanisms of trace-element uptake in these regions. Li, Mg, U and Sr exhibited noticeable and reproducible offsets within the inner skeletal area surrounding the hollow central axis of all *Keratoisis* sp. internodes examined here, with the outer internode wall depleted in Mg and Li and enriched in U (Fig. 1). Both modern and fossil bamboo corals species do not demonstrate centres of calcification (Noé and Dullo,

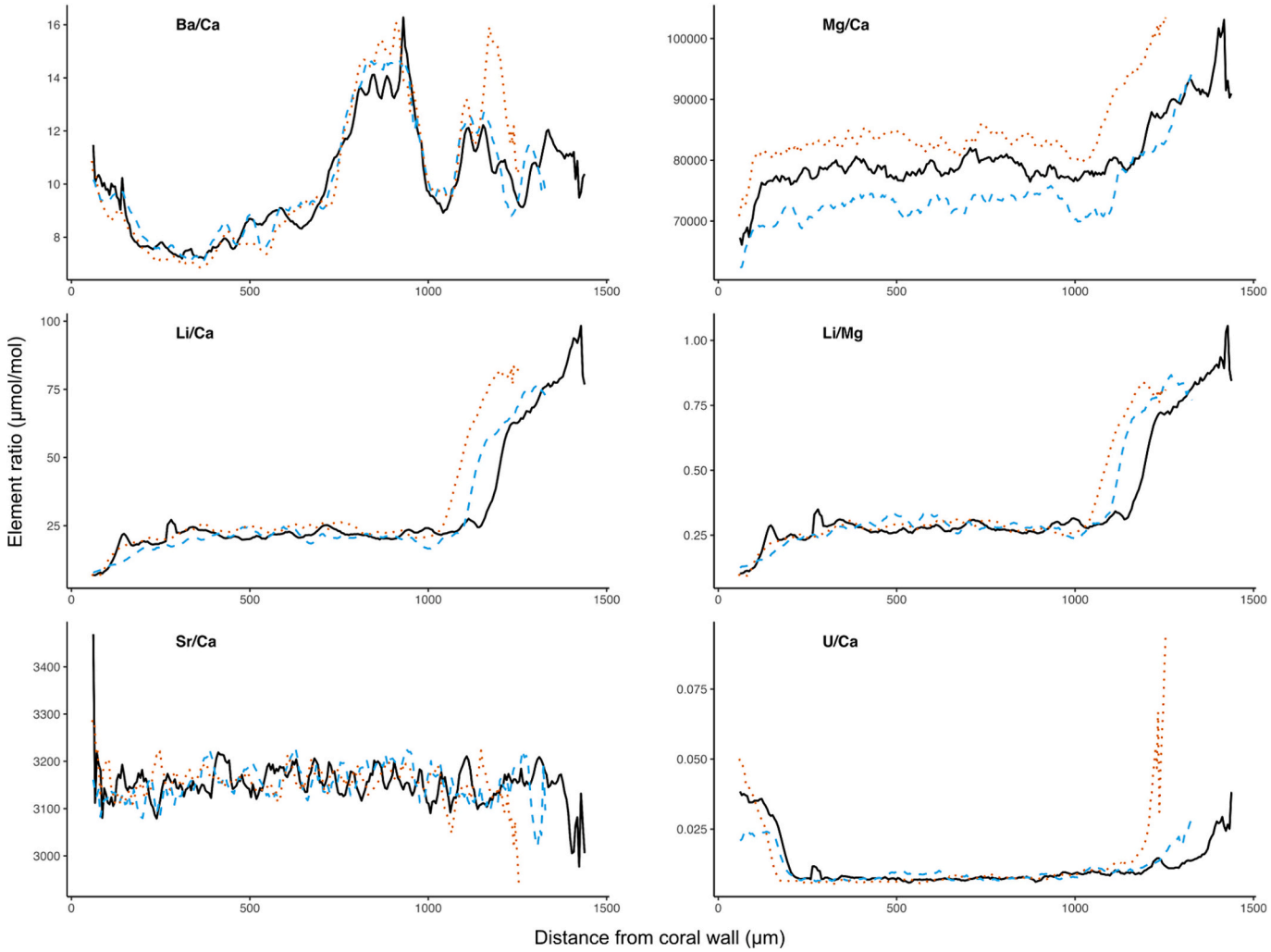

Fig. 3. Summary of tuning stratigraphic element signals for *Keratoisis* sp. colony (a) #23–1, (b) #23–6, (c) #23–10, and (d) #23–16. In each panel, tuning stratigraphic trace element signals (y-axis) carried out in QAnalyseries (v 1.5.1, Kotov and Pälike, 2018) are presented across basal (**black solid line**), second (**dotted blue line**) and third (**dashed orange line**) internodes. (For interpretation of the references to colour in this figure legend, the reader is referred to the web version of this article.)

2006). Instead, the skeletal region encompassing the hollow central axis has been previously inferred as product of secondary infilling by amorphous carbonate as the colony grows (Noé and Dullo, 2006), although this feature is not shared among all bamboo coral taxa (Thresher et al., 2004; Andrews et al., 2009; Thresher et al., 2010; Farmer et al., 2015b). Faster growth rates in this inner band may cause elevated Mg/Ca via enhanced Mg partitioning at higher calcite precipitation rates – an explanation supported by other studies of *Keratoisis* spp. (Sinclair et al., 2011; Thresher et al., 2016; Thresher and Neil, 2016; Flöter, 2019; Flöter et al., 2019, 2022). The outer edge of all the *Keratoisis* sp. internodes examined here is a more porous, presumably ontogenetically younger calcite band (Fig. 1) which at some stage as coral matures, must transform to be the same density and geochemical composition as the central section. This implies there are at least two stages of growth for *Keratoisis* skeleton: the initial deposition of a low-density outer band (Williams et al., 2024) that matures, gaining Mg, Li and losing U and increasing in density as it is encompassed by further growth. To the best of our knowledge, the details of this process has not been described for the outer band of bamboo coral internodes. However, Flöter et al. (2019) describes an infilling process occurring within fan-shaped pits after calcite mineralisation around desmocytes in *Keratoisis grayi*. The occurrence of secondary infilling within the outer band remains speculative without a more detailed view on internode micro-architecture, but as this feature is prominent in adjacently sampled colonies of *Keratoisis* sp. and within multiple internodes of the same specimen, it is clearly a consistent feature of this species. If our interpretation of this feature is correct, it implies that the trace element content of the central mature section of skeleton is dependent on how much of the skeleton was deposited as the immature, porous outer band versus how much was obtained secondarily. Given the scale of the variations in composition we observe (Fig. 1), this process would influence Mg, Li and U, more than Ba and Sr (Fig. 3). The relationship between temperature and Mg in this bamboo coral is, thus, likely to be influenced by when the skeleton is deposited, a currently rather poorly constrained vital effect. Additionally, this two-stage calcification process suggests that any given layer in the skeleton calcified over multiple years, integrating environmental signals. Using the age model and the distance over which the anomalous Mg signals occur (80 to 225 µm, dependant on the size of the specimen), we estimate this temporal averaging to be over at least 1.6 (#23–10) to 4.4 (#23–6) years, respectively. Irrespective of the underlying mechanisms driving the alteration in mineralisations, we suggest that the immature, outer porous calcite and the potentially faster growing inner band surrounding the central axis should be excluded when using the Mg/Ca-temperature

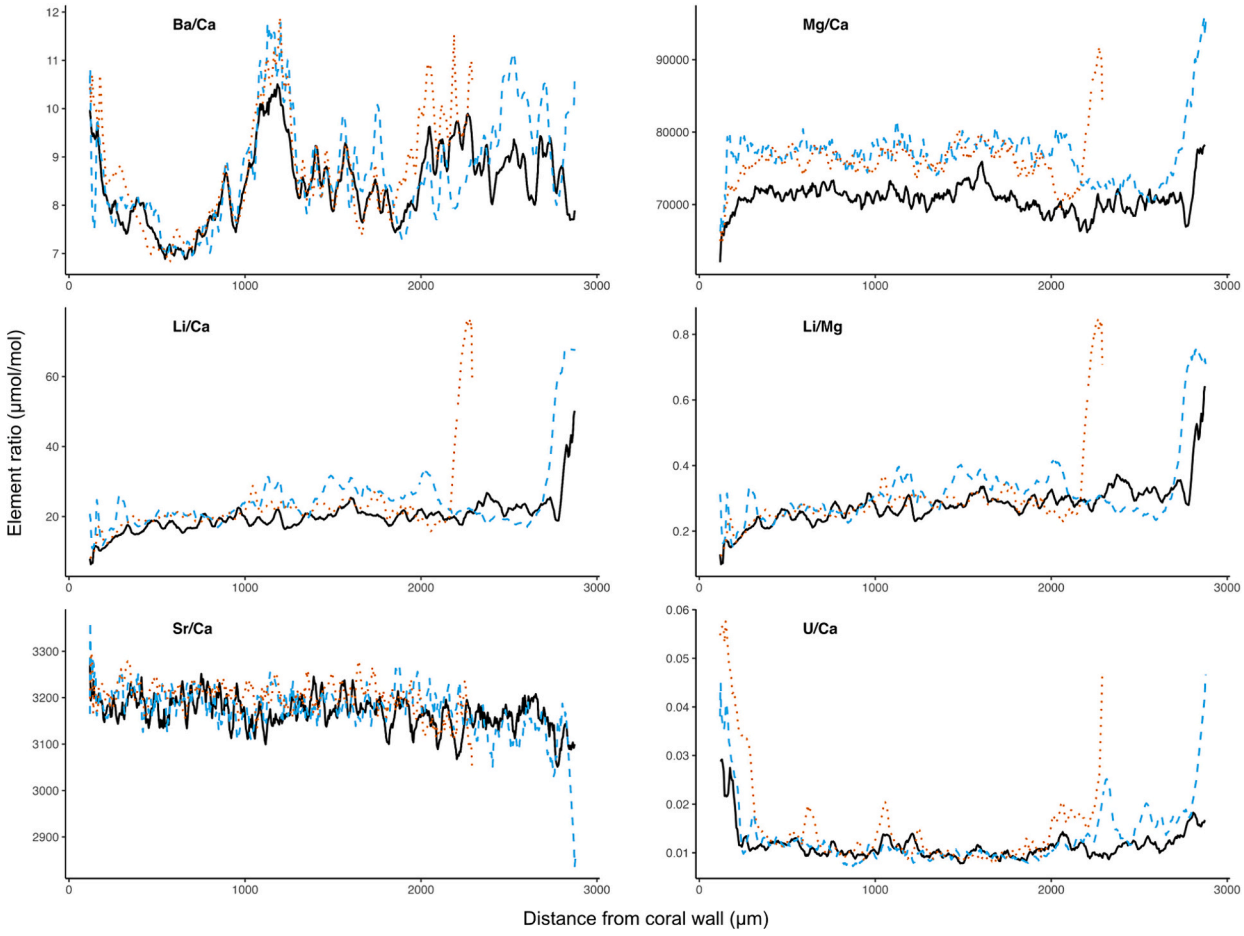

Fig. 3. (*continued*).

proxy in *Keratoisis* sp.

4.1. Multi-taxa element analysis

4.1.1. Mg/Ca

The cross-study comparison of multi-taxa calibrations demonstrates a strong positive Mg/Ca temperature relationship in high-Mg calcitic Octocorals found between −2 to 27 °C (Fig. 4a). Mg/Ca temperature sensitivity is well documented in several gorgonian families (Weinbauer et al., 2000; Sherwood et al., 2005b), albeit with taxon-specific slopes and intercepts (Sinclair et al., 2011; Thresher et al., 2009). The calibration slope utilised here (0.316 ± 0.026 °C/mmol/mol), which integrates 91 datapoints from four separate investigations (supplementary material Data Record S1), is in line with previous gorgonian calculations (Thresher et al., 2016) but has a tighter distribution of residuals, with 87% of bulk Mg/Ca explained by ambient temperature. Here, we observe differences in average Mg/Ca within and between individuals of *Keratoisis* sp. (Fig. 4), leading to variable offsets in paleotemperature reconstructions from in-situ temperature measurements when using a SubClass-level calibration. Whilst we could have opted for a calibration specific to the *Keratoisidinae* SubFamily, it would have resulted in a substantially weaker regression and flatter gradient ([T °C] = 0.12 ± 0.08 [Mg/Ca mmol/mol] – 6.64 ± 6.63; $R^2 = 0.13$) calculated over a smaller range of temperatures (−1.9 to 10 °C) with 95% confidence intervals of ±10 °C. As such, despite the offsets within individuals of *Keratoisis* sp., the robustness of the linear calibration model derived from the combined Octocoral data instils confidence in the suitability of Mg/Ca for estimating past temperatures.

4.1.2. Ba/Ca

Superficially, bulk Octocoral Ba/Ca also appears to be related to in-situ temperature, much like other taxon- and mineralogy-specific relationships (Fig. 4b). However, similar studies on other cold-water species demonstrate a strong covariance between $[Ba]_{SW}$ and T (Scleractinia, Spooner et al., 2018), and a relatively minor dependence on coral Ba/Ca on T has been reported in a warm water species (*Favia fragum*, Gonneea et al., 2017). Here, Ba/Ca values for *Keratoisis* sp. colonies fall outside of the linear relationship with temperature, implying that the correlation between Ba/Ca and temperature in Octocorals is predominantly driven by non-thermal effects (LaVigne et al., 2011; Thresher et al., 2016, Flöter et al., 2019; Geyman et al., 2019). This is important because a dependence of Ba/Ca on $[Ba]_{SW}$, for example, could provide an insight into the dynamics and circulation of refractory nutrients from the overlying water column (Chow and Goldberg, 1960; Wolgemuth and Broecker, 1970).

The inclusion of our specimens in the Octocoral Ba/Ca versus $[Ba]_{SW}$ calibration improves on the well-defined, linear relationship in LaVigne et al. (2011) for the *Keratoisididae* family, and now encompasses 9 different ecoregions of the globe (supplementary material, Dataset S1): [Ba/Ca µmol/mol] = 0.148 ± 0.005 [Ba_{SW} nmol/kg], $R^2 = 0.97$, $p < 0.001$ (Fig. 4b). This relationship also overlaps with that previously demonstrated for high-Mg Stylasterids (Kershaw et al., 2023; Table 5), assuming that the only source of Ba to the skeleton is from the dissolved pool in seawater (i.e. if $[Ba]_{SW} = 0$, then the coral skeleton Ba/Ca ratio = 0). However, we find evidence of ontogenetic variability in D_{Ba} for *Keratoisis* (Fig. 4b), indicating that such an assumption may be incorrect due to differences in the controls on D_{Ba} between colonies, in addition to genus-level vital- and/or site-specific effects (Flöter et al., 2019).

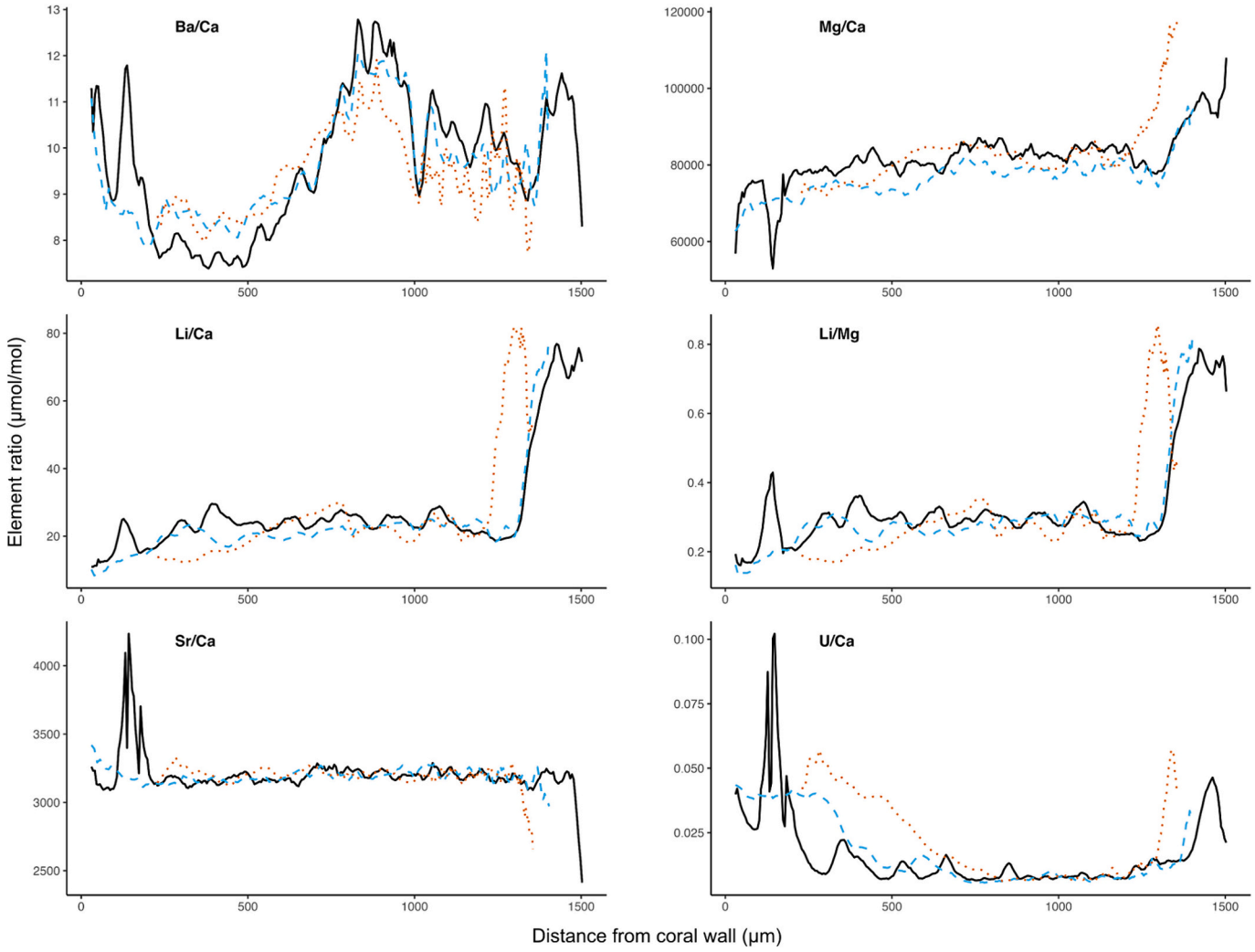

Fig. 3. (*continued*).

Furthermore, we acknowledge the caveat on comparing to extrapolated $[Ba]_{SW}$, which is a less accurate estimation than taking proximal seawater measurements at the point of coral sampling. Regardless, the empirically calibrated model of Ba/Ca vs $[Ba]_{SW}$ that emerges from the combined Octocoral data (Table 5) appears to be robust, despite the inclusion of different genus and methodologies for obtaining seawater barium measurements, providing confidence in its applicability to estimate past $[Ba]_{SW}$.

4.2. Microscale element discrepancies

When interpreting any palaeoceanographic record it is important to consider the fidelity with which a proxy can reproduce the hydrographic parameter of choice. When using the Octocoral derived calibration, Mg/Ca values in our *Keratoisis* sp. colonies suggest a maximum temperature variability of ±3.78 °C across the timeframe common to all colonies and maximum prediction uncertainty of ±4.52 °C when reconstructing temperature for any given timepoint. This exceeds the temperature variability documented at parallel depths achieved during long-term monitoring across the Davis Strait (Curry et al., 2011), the entire Baffin Bay basin (Zweng and Münchow, 2006; Birch et al., 1983), and even proximate deep-water CTD casts from the past three years (pers. comm., Azetsu-Scott). One explanation might be that the newly refined multi-taxa calibration, which uses globally distributed Octocoral colonies derived from multiple water depths, is not appropriate for *Keratoisis* sp. and/or for our high-resolution Mg/Ca mapping approach. An alternative explanation is that this species' enhanced reconstructed temperature variability reflects variable physiological processes that influence Mg-uptake rather than issues relating to calibration (Flöter et al., 2019, Sinclair et al., 2011, Thresher et al., 2010, Thresher et al., 2016; Section 5). If the latter is the case, biological variability exerts a major control on the ability of this species to accurately preserve environmental information, but it is unclear whether these inter- and intra-colony offsets differ from site to site or represent an intrinsic feature of this species of *Keratoisis* as is it poorly characterised by available studies.

4.2.1. Variation within and between individuals

Observations of element signals across internodes reveal asynchronous variability between E/Ca transects, indicating that variability in contemporaneous skeletal composition is large enough to adjust paleoenvironmental reconstructions that are based on sub-annual, annual and interannual element chronologies even after stratigraphic tuning. The examination of replicate E/Ca transects per analysed colony can assist in unravelling the influence of environmental factors versus physiological effects (Sinclair et al., 2011; DeLong et al., 2007; Kawakubo et al., 2014) and is demonstrated here by leveraging the data from different internodes into a singular timeline, which reduced the prediction uncertainty of seasonally interpolated and annually interpolated temperature reconstruction by an average of 55% and 48%, respectively. However, it is important to exercise caution when predicting seawater conditions, as

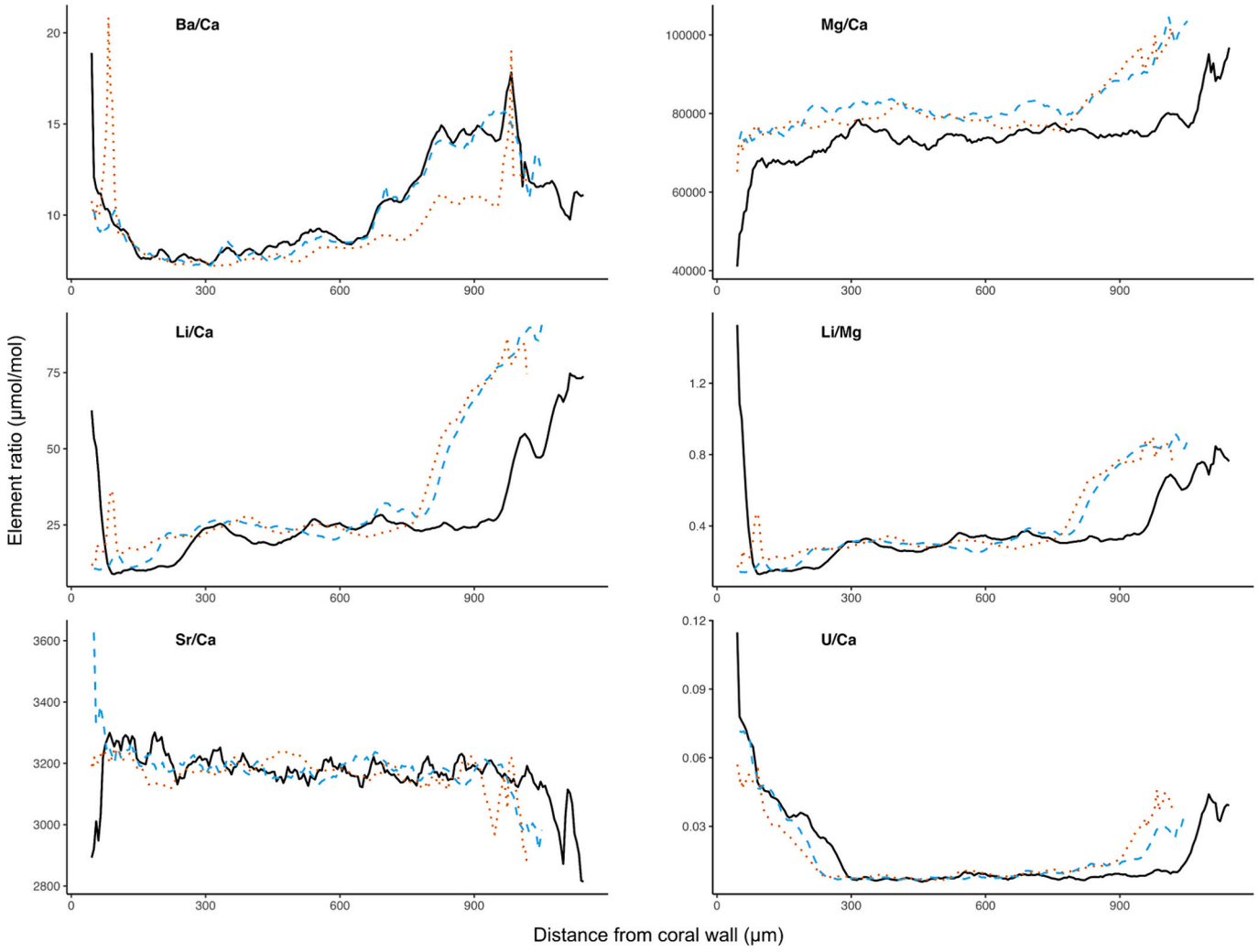

Fig. 3. (*continued*).

this approach primarily assesses the consistency of the relationship within living proxy carriers. Enhancing accuracy requires in-situ measurements to adjust the linear or non-linear regression between the coral's element proxy and the environmental variable of interest. This is regularly employed in tropical (Hu et al., 2018; Cuny-Guirriec et al., 2019; Hathorne et al., 2013) and temperate (Montagna et al., 2014) coral studies due to the abundance of hydrological stations, buoys, and satellite information within these regions.

Though long-term reconstructed T and $[Ba]_{SW}$ variability is very coherent across the coral colonies, most sub-annual fluctuations occurred at different timepoints, suggesting that ontogenetic variation between colonies collected from the same location can influence paleoenvironment reconstructions at seasonal resolution and below. As physical conditions tend to coalesce with depth (Rogers, 2015) we contend that the interannual and sub-annual variations of *Keratoisis*-derived temperature and $[Ba]_{SW}$ is unlikely to be driven by localised oceanographic variability (Fig. 5). Where small-scale environment fluctuations cannot solely explain coral element variability, vital effects are considered the main contributor in high-Mg bamboo corals (Sinclair et al., 2011; Hill et al., 2011; Robinson et al., 2014; Flöter et al., 2019) and are also present in the *Keratoisis* sp. colonies examined here, with several mechanisms (Rayleigh fractionation, ion-specific pumping, and Ca/proton exchange) investigated to explain the distribution of Na and S (Flöter et al., 2022). To better understand the differences in element behaviour across growth lines in coral colonies, there is a requirement to investigate the controlling mechanisms of element uptake in regions where patterns diverge from what would be expected when solely driven by environmental influences; in the *Keratoisis* sp. colonies examined here, for example, this would refer to the inner and outer bands of the internodes. This could involve examining the effects of non-linear growth rates (Sinclair et al., 2011; Farmer et al., 2015b) on element incorporation in *Keratoisis* and other bamboo coral species under varying environmental conditions to establish more robust chronologies, as growth rates are known to vary within modern (Sinclair et al., 2011; Thresher et al., 2016; Thresher and Neil, 2016; Flöter, 2019; Flöter et al., 2019, 2022) and fossilised (Noé et al., 2008) individuals of other *Keratoisis* spp.. This, along with revised calcification models, can help predict element behaviour, disentangle environmental influences from the physiological drivers of calcitic skeletal composition (Flöter et al., 2022) and, therefore, enable confident exploration of environmental reconstructions at finer temporal resolutions.

4.2.2. Sr/Ca, U/Ca, and Li/Mg in high-Mg calcitic Octocorallia

Environmental effects on Sr/Ca values are known to vary between gorgonian taxa (Weinbauer and Velimirov, 1995; Heikoop et al., 2002) and in other bamboo coral species track seawater Sr/Ca ratios rather than temperature (Hill et al., 2012). We are not aware of any studies that have explored the Li/Mg temperature relationship in high-Mg cold water Octocorals (Fig. 4; supplementary material, Dataset S1), but it does not reflect temperature in warm water counterparts (*Corallium*

Table 4
Correlation scores (Pearson's) for element ratio patterns after stratigraphic tuning internodes 1 & 2 and internodes 1 & 3 for each colony and their combined mean (bold).

Element ratio	Colony ID	Internode	Correlation after tuning
Ba/Ca	#23–1	1 & 2	0.953
		1 & 3	0.956
	#23–10	1 & 2	0.840
		1 & 3	0.713
	#23–16	1 & 2	0.971
		1 & 3	0.614
	#23–6	1 & 2	0.750
		1 & 3	0.903
	Mean	**1 & 2**	**0.879**
		1 & 3	**0.797**
Li/Ca	#23–1	1 & 2	0.923
		1 & 3	0.869
	#23–10	1 & 2	0.964
		1 & 3	0.113
	#23–16	1 & 2	0.660
		1 & 3	0.410
	#23–6	1 & 2	0.618
		1 & 3	0.258
	Mean	**1 & 2**	**0.791**
		1 & 3	**0.413**
Li/Mg	#23–1	1 & 2	0.907
		1 & 3	0.854
	#23–10	1 & 2	0.943
		1 & 3	0.042
	#23–16	1 & 2	0.438
		1 & 3	0.123
	#23–6	1 & 2	0.610
		1 & 3	0.320
	Mean	**1 & 2**	**0.725**
		1 & 3	**0.335**
Mg/Ca	#23–1	1 & 2	0.895
		1 & 3	0.829
	#23–10	1 & 2	0.814
		1 & 3	0.029
	#23–16	1 & 2	0.623
		1 & 3	0.553
	#23–6	1 & 2	0.513
		1 & 3	0.296
	Mean	**1 & 2**	**0.711**
		1 & 3	**0.427**
Sr/Ca	#23–1	1 & 2	0.022
		1 & 3	0.275
	#23–10	1 & 2	−0.012
		1 & 3	0.489
	#23–16	1 & 2	−0.208
		1 & 3	0.032
	#23–6	1 & 2	0.343
		1 & 3	0.237
	Mean	**1 & 2**	**0.036**
		1 & 3	**0.258**
U/Ca	#23–1	1 & 2	0.811
		1 & 3	0.568
	#23–10	1 & 2	0.680
		1 & 3	0.624
	#23–16	1 & 2	0.913
		1 & 3	0.763
	#23–6	1 & 2	0.834
		1 & 3	0.786
	Mean	**1 & 2**	**0.810**
		1 & 3	**0.685**

rubrum; Chaabane et al., 2019). Interestingly, U/Ca demonstrated high reproducibility at the micrometre scale in *Keratoisis* sp. and a significant relationship with seawater temperature across high-Mg Octocorals is observed in other studies (Fig. 4). However, the U/Ca proxy in Octocorals is extremely sensitive (Table 5a) and inverse to what is observed in the aragonitic coral literature data (Fig. 4; Armid et al., 2011). Few studies have directly compared the utility of the range of available temperature proxies (U/Ca, Sr/Ca, Li/Mg, and Sr—U) at sub-annual resolution (e.g. Ross et al., 2019) or across overlapping growth periods within the same colony, so whether temperature sensitivity of U/Ca is universal across taxa is unknown.

4.3. Prospect for a E/Ca paleothermometer in Keratoisis sp.

Temperature reconstructions over the shared timeframe for all colonies reveal a notable, but minor cooling trend in deep-water during the past 20 years (Fig. 5a). The accuracy of this reconstruction is challenging to determine due to the lack of complete continuous in-situ temperature datasets but, acknowledging the caveat of comparing deep water observations to a surface temperature dataset, it is comparable to trends observed in local OISST (Fig. 5a). When considering the entire 20th century, a gradual warming trend has been observed in the deep-water layer of the Baffin Bay basin (Zweng and Münchow, 2006; Birch et al., 1983) most likely caused by an increase in temperature of the inflowing Atlantic waters of the West Greenland Current. This speculative conclusion is supported by the existence of a correlation of subsurface (~900 m) temperature fluctuations with the NAO over the same timeframe (Zweng and Münchow, 2006). As Baffin Bay is a semi-enclosed basin to the north of the Labrador Sea, any hydrographic changes here may indicate potential climate shifts because water exiting Baffin Bay enters the Labrador Sea, one of the two/three deep convection sites in the Northern Hemisphere (Pickart et al., 2002, 2003). Though all available in-situ measurements pre-date 2003 and are outside the timeframe of this study, the deep-water warming trend (OLS regression ±95 CI) determined from sporadic bottle- and CTD-casts within a 200 m vertical bin (1967–1998, 800–1000 m, $n_T = 10$; 0.016 ± 0.013 °C/yr; Zweng and Münchow, 2006) is smaller than the Mg/Ca reconstructed temperature trend (annual interpolated) obtained from our longest-lived colony as determined over the same timeframe (averaged over internodes, $n_T = 31$, 0.060 ± 0.017 °C/yr; Fig. 6). As both the coral and direct measurements demonstrate overlapping trends in temperature, this provides confidence in the derived relationship between Mg/Ca of *Keratoisis* sp. and ambient temperature, but perhaps points to the relationship between Mg/Ca vs. T, as defined by the existing literature (Fig. 4), as being too shallow. Nonetheless, improving the precision of this proxy is necessary before wider application as, even when leveraging replicate transects, the external error of our current Mg/Ca method corresponds to roughly 2 °C when using the slope of the relationship between Mg/Ca and temperature for high-Mg calcitic Octocorals. Additionally, vital effects inside both the younger, porous, outer band, and the inner band surrounding the central axis of internodes, are still likely to present a challenge to the development of a Mg/Ca paleothermometer that is captured over the entire lifespan of *Keratoisis* sp. colonies. Nevertheless, as Mg/Ca in the mature central section of the internodes exhibits low variance, and accepting the limitations of analytical error, we remain confident that regional analyses in the future are likely to yield an improved test of a Mg /Ca deep-sea cold-water paleothermometer as more in-situ temperature data becomes available.

4.4. Prospect for a nutrient tracer in Keratoisis sp.

The existence of Ba/Ca variability in coral skeletons related to variability in $[Ba]_{SW}$ is well documented in bamboo corals (LaVigne et al., 2011). The consistent Ba enrichment seen across all corals here indicates that the driving factor behind these peaks extends beyond their immediate environment, suggesting they truly reflect changes in $[Ba]_{SW}$. The peaks themselves tend to be broad, indicating either slow changes in $[Ba]_{SW}$ that perhaps relate to the prolonged input of Ba to the seafloor, or a broadening of quite sharp peaks by the skeletal maturation process described in Section 5. Despite the corals not being coastal, they inhabit a sizable submarine sedimentary trough-mouth fan adjacent to Disko Bay, which has experienced historical meltwater sediment delivery (Ó Cofaigh et al., 2018). This suggests that large-scale variations in Ba content of riverine/meltwater inputs might be responsible for the Ba peaks (Sinclair and McCulloch, 2004; Sinclair et al., 2011). However, it

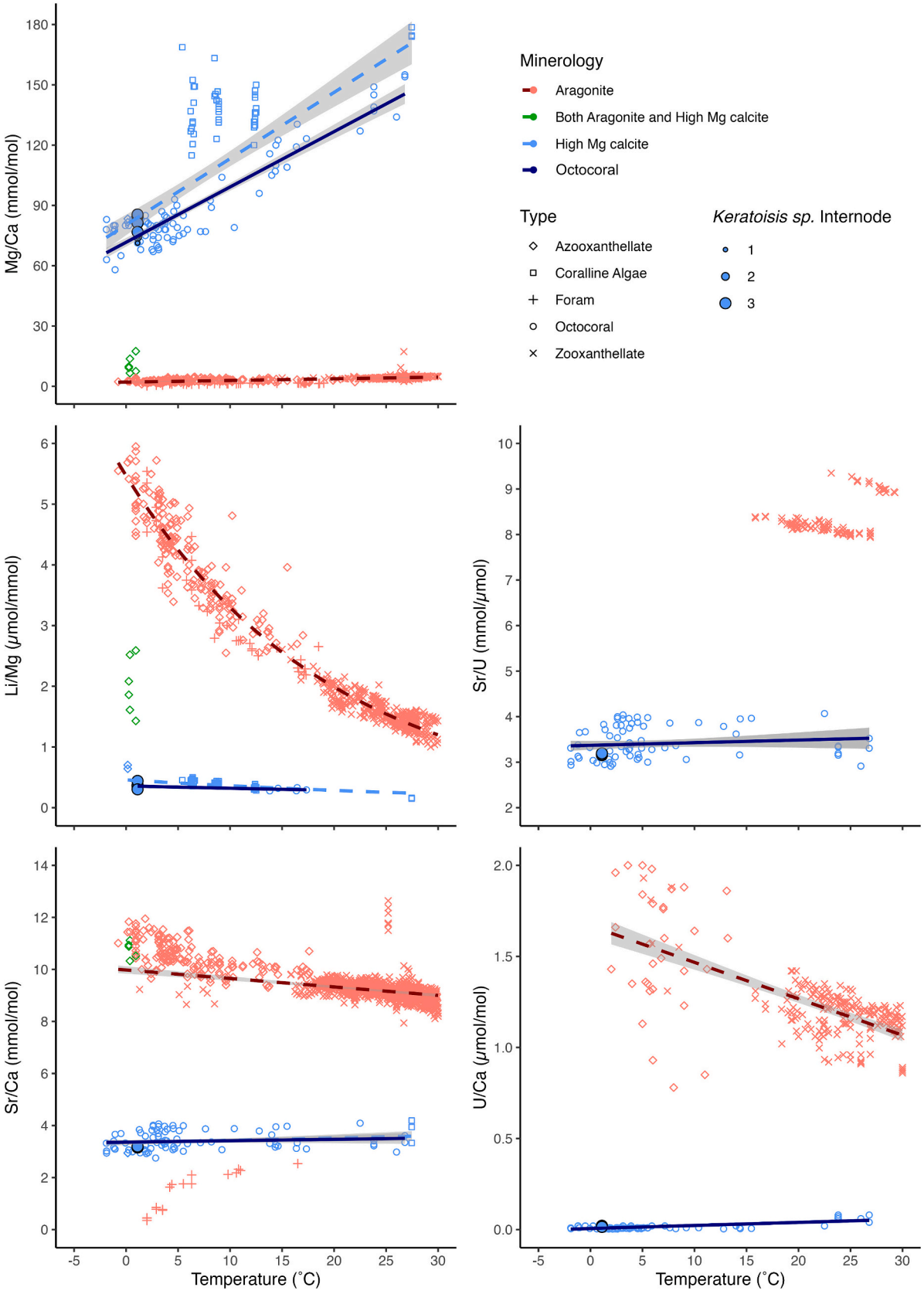

Fig. 4. Compiled published (a) Mg/Ca – T, Li/Mg – T, Sr/Ca – T, Sr/U – T and U/Ca – T calibration data and (b) for aragonitic (**red points, dark red line**), high-Mg calcitic (**blue**) mixed mineralogy (**green**) corals and Corallinales compared to Octocorallia (**dark blue line**). Full element compilation datasets adjusted for interlaboratory offsets (where standard data are available). Average error bar is shown for *Keratoisis* sp. $[Ba]_{SW}$ and D_{Ba}. Mean coral replicates are presented in the electronic supplementary material Dataset S1. (For interpretation of the references to colour in this figure legend, the reader is referred to the web version of this article.)

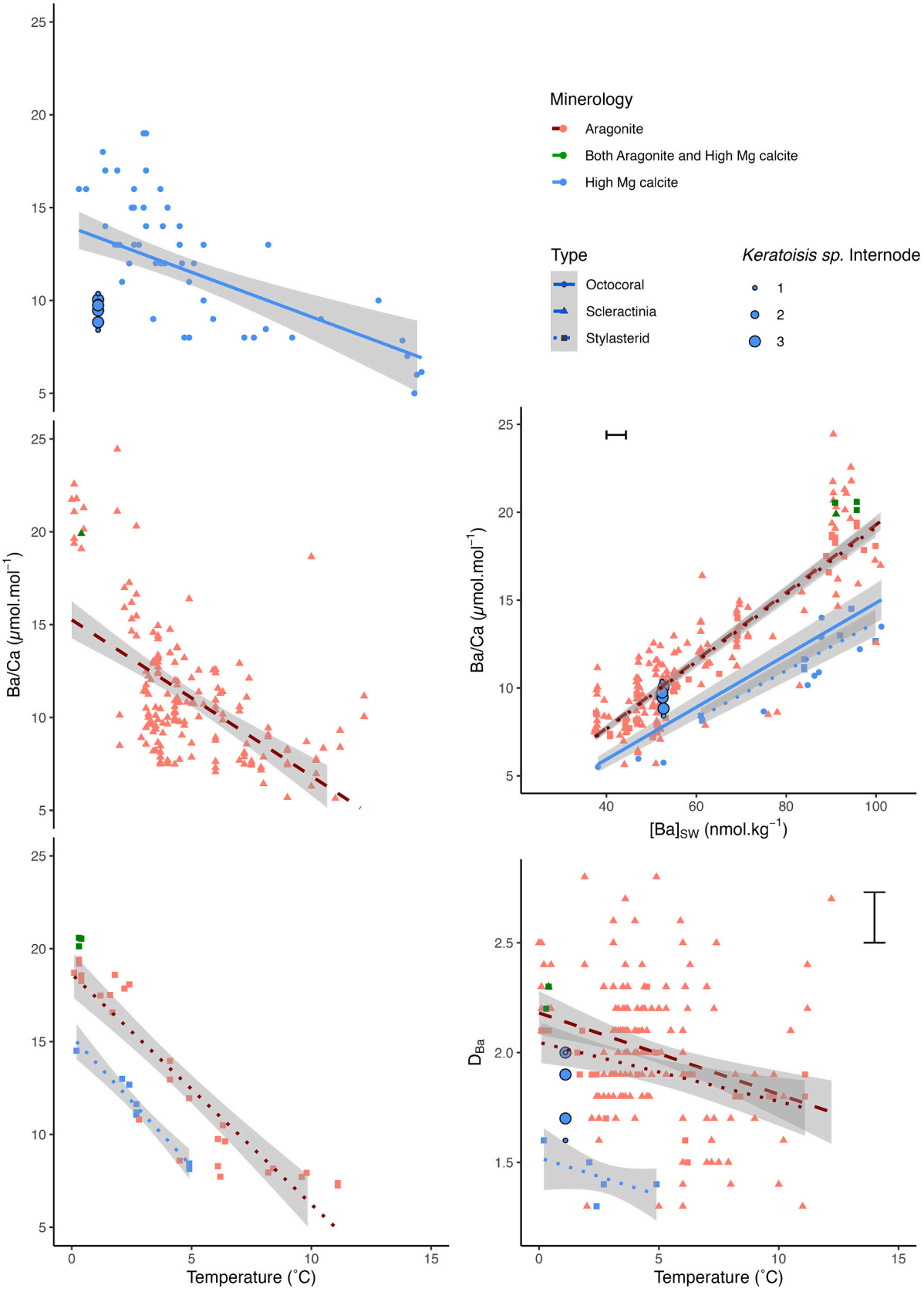

Fig. 4. (*continued*).

is important to consider the compositions of other inputs, such as groundwaters, submarine discharge, sea-ice, and snowpack. Meteoric water, primarily glacial meltwater from the Greenland Ice Sheet, is the dominant source of freshwater in the Davis Strait region (Azetsu-Scott et al., 2012), from which barium bound to transported particulates is likely to sink towards the deep water. Although limited ice discharge

Table 5
(a) Linear and (b) Non-linear calibration Ordinary Least Squares (OLS) and Reduced Major Axis (RMA) equations based on values extracted from the literature and published calibrations with >60% variance explained (bold). All published equations extracted from the literature and the 53 data sources can be found in the supplementary material Dataset S1.

(a)

Relationship	*x unit*	*y unit*	*Mineralogy*	*Taxon Group*	*Source*	*n*	*r*	R^2	*Type of regression*	*p*	*Gradient*	*± 2SD*	*Intercept*	*± 2SD*
[Ba]SW ~ Ba/Ca + 0	µmol/mol	nmol.kg	**Aragonite**	***Scleractinia***	**Multiple studies**	**172**		**0.97**	**OLS**	**0.001**	**5.040**	**0.065**		
				Stylasteridae	Kershaw et al., 2023	**28**		**0.99**	**OLS**	**0.001**	**5.190**	**0.073**		
			High-Mg calcite	**Octocorallia**	**Multiple studies**	**45**		**0.97**	**OLS**	**0.001**	**6.530**	**0.237**		
				Stylasteridae	Kershaw et al., 2023	**8**		**0.99**	**OLS**	**0.001**	**7.260**	**0.169**		
			Aragonite	***Scleractinia***	Anagnostou et al., 2011	**17**		**0.60**	**OLS**		**1.400**	**0.300**	**0**	**2**
Temperature ~ Ba/Ca	µmol/mol	°C	**Aragonite**	*Scleractinia*	Multiple studies	174	−0.58	0.34	OLS	0.001	−0.394	0.082	9.272	0.974
									RMA	0.001	−0.690	0.163	12.590	1.464
				Stylasteridae	Kershaw and et al., 2023	**28**	**−0.92**	**0.85**	**OLS**	**0.001**	**−0.682**	**0.118**	**13.383**	**1.649**
									RMA	**0.001**	**−0.729**	**0.135**	**14.005**	**1.561**
			High-Mg calcite	Octocorallia	Multiple studies	91	−0.73	0.54	OLS	0.001	−1.332	0.260	21.082	3.105
									RMA	0.001	−1.863	0.409	27.056	3.706
				Stylasteridae	Kershaw and et al., 2023	**8**	**−0.98**	**0.95**	**OLS**	**0.001**	**−0.680**	**0.154**	**10.525**	**1.770**
									RMA	**0.001**	**−0.696**	**0.177**	**10.709**	**1.621**
Temperature ~ Dba	–	°C	Aragonite	*Scleractinia*	Multiple studies	172	−0.22	0.05	OLS	0.004	−1.682	1.110	8.173	2.245
									RMA	0.004	−12.163	17.925	29.086	10.849
				Stylasteridae	Kershaw and et al., 2023	28	−0.55	0.30	OLS	0.003	−11.121	6.863	25.818	13.288
									RMA	0.003	−27.149	35.099	56.730	22.137
			High-Mg calcite	*Stylasteridae*	Kershaw and et al., 2023	8	−0.59	0.34	OLS	0.061	−10.091	13.904	17.205	19.846
									RMA	0.061	−18.345	395.398	28.966	23.548
Temperature ~ Mg/Ca	mmol/mol	°C	Aragonite	All taxon	Multiple studies	576	0.67	0.45	OLS	0.001	5.419	0.487	−1.862	1.816
									RMA	0.001	11.581	0.957	−23.500	4.004
			High-Mg calcite	**All taxon**	**Multiple studies**	**93**	**0.93**	**0.87**	**OLS**	**0.001**	**0.317**	**0.026**	**−22.065**	**2.361**
									RMA	**0.001**	**0.345**	**0.027**	**−24.467**	**2.615**
				Octocorallia	**Multiple studies**	**91**	**0.93**	**0.87**	**OLS**	**0.001**	**0.316**	**0.026**	**−21.881**	**2.336**
									RMA	**0.001**	**0.342**	**0.027**	**−24.173**	**2.576**
			High-Mg calcite	**Corallinales**	Hetzinger et al., 2018	**164**	**0.88**		**OLS**	**0.001**	**0.345**	**0.015**	**−41.834**	**2.163**
Temperature ~ Li/Mg	µmol/mmol	°C	High-Mg calcite	Octocorallia	Multiple studies	17	−0.55	0.30	OLS	0.008	−82.140	68.650	33.180	23.410
									RMA	0.008	−201.280	104.020	73.460	210.440
Temperature ~ Sr/Ca	mmol/mol	°C	Aragonite	All taxon	Multiple studies	2013	−0.24	0.06	OLS	0.001	−1.813	0.315	39.509	2.922
									RMA	0.001	−26.228	5.501	264.986	35.916
			High-Mg calcite	All taxon	Multiple studies	92	0.14	0.02	OLS	0.094	3.041	4.540	−4.339	15.440
									RMA	0.094	25.060	24.324	−78.853	−675.793
				Octocorallia	Multiple studies	90	0.12	0.01	OLS	0.137	2.643	4.662	−2.890	15.900
									RMA	0.137	28.456	30.297	−90.495	−286.162
			High-Mg calcite	**Corallinales**	Kamenos et al., 2008		**0.88**	**0.77**	**OLS**	**0.001**	**3.137**	**0.166**	**−2.060**	**0.730**
Temperature ~ Sr/U	mmol/mol	°C	Aragonite	All taxon	Multiple studies	103	0.45	0.20	OLS	0.001	4.106	1.610	−10.980	13.421
									RMA	0.001	8.068	2.790	−43.969	31.770
			High-Mg calcite	Octocorallia	Multiple studies	81	0.13	0.02	OLS	0.121	2.704	4.795	−3.652	16.393
									RMA	0.121	9.525	16.353	−26.856	99.647
			Aragonite	**All taxon**	Ross et al., 2019	**33**		**0.89**	**OLS**	**0.001**	**−0.035**		**8.920**	
Temperature ~ U/Ca	µmol/mol	°C	Aragonite	All taxon	Multiple studies	245	−0.72	0.52	OLS	0.001	−18.913	2.297	45.241	3.022
									RMA	0.001	−32.525	4.414	62.650	4.579
			High-Mg calcite	Octocorallia	Multiple studies	81	0.75	0.56	OLS	0.001	334.277	66.002	0.500	1.471
									RMA	0.001	472.536	83.521	−1.587	1.612
			Aragonite	***Porites cylindrica***	Armid et al., 2011			**0.78**	**OLS**		**−0.021**	**0.002**	**1.488**	**0.048**

(b)

Relationship	*x unit*	*y unit*	*Mineralogy*	*Taxon Group*	*Source*	*n*	*a*	*p*	*± SE*	*b*	*p*	*± SE*
Li/Mg ~ $a*e^{[b*Temperature]}$	°C	µmol/mmol	Aragonite	All taxon	Multiple studies	597	5.469	0.001	0.030	−0.051	0.001	0.000
			High-Mg calcite	All taxon	Multiple studies	59	0.458	0.001	0.019	−0.046	0.001	0.005
			Aragonite	**All taxon**	Montagna et al., 2014	**49**	**5.41**			**−0.05**		**0.002**
			High-Mg calcite	**All taxon**	Stewart et al., 2020	**49**	**0.63**		**0.02**	**−0.05**		**0.002**

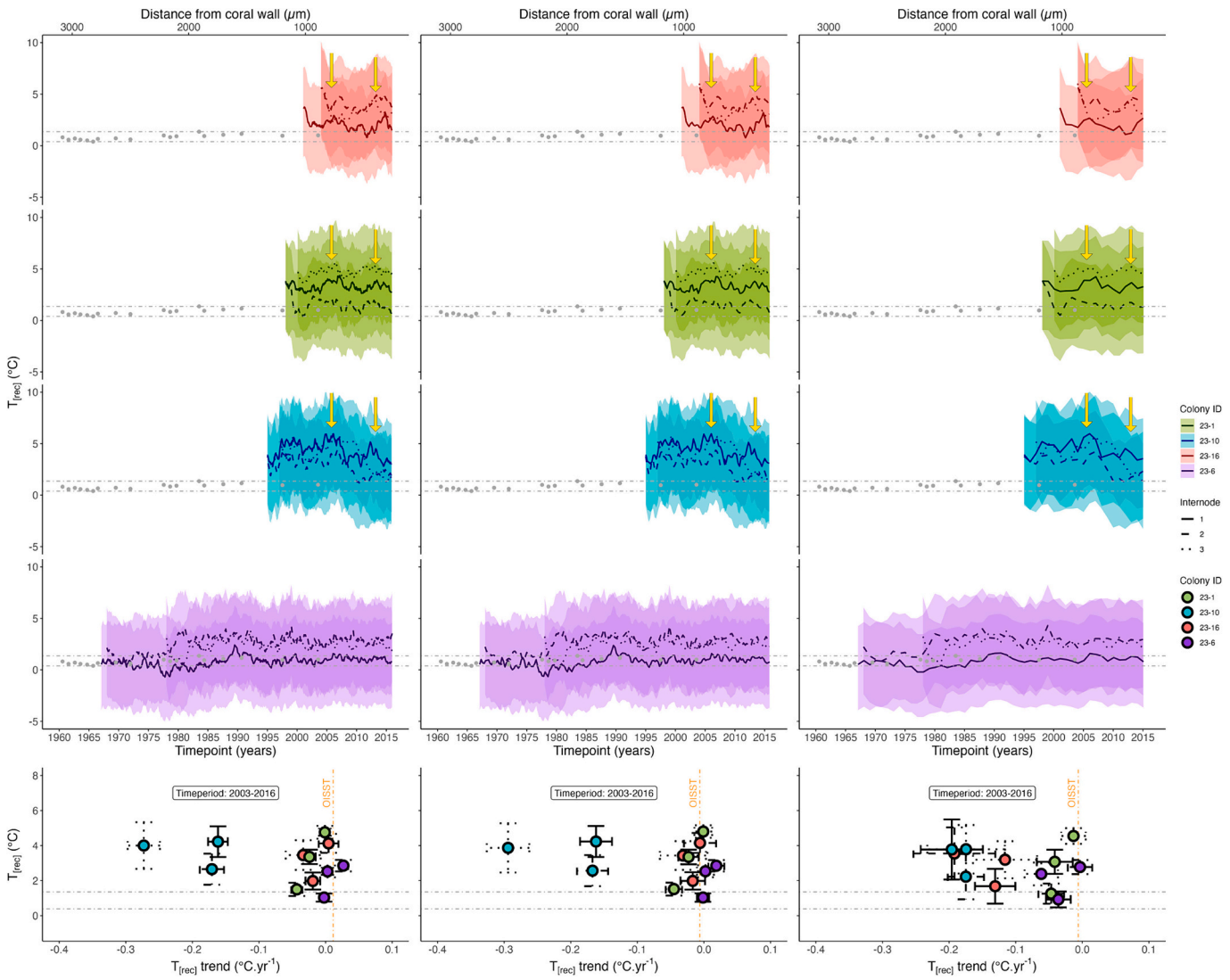

Fig. 5. Reconstructions of past (*a*) temperatures derived from Mg/Ca and (*b*) seawater barium derived from Ba/Ca, generated for different colonies (**colour**) and internodes (**linetype**) and evaluated without data interpolation (**left column**), with seasonal interpolation (**middle column**), and with annual interpolation (**right column**). In-situ environmental measurements taken at nearby locations (**grey points and dash-dot lines** - temperature: K. Azestu-Scott, pers. comm., May 31, 2022; Zweng and Münchow, 2006; $[Ba]_{SW}$: Thomas et al., 2021) and the average trend of sea surface temperatures (**dashed yellow line**, Reynolds et al., 2002) are displayed. Synchronised multi-annual cycles in the basal internodes are highlighted with arrows. The bottom row of each figure shows the reconstructed environmental conditions during the time period shared by all *Keratoisis* sp. colonies. (For interpretation of the references to colour in this figure legend, the reader is referred to the web version of this article.)

data prior to 2000 is available, a noticeable increase in ice discharge (particularly from the Jakobshavn Glacier flowing into the Disko Bay region) is observed during the early 21st century and from 2012 to 2015 (Mankoff et al., 2020). The observed increase in barium concentrations towards the outermost portion of our coral records is in agreement with this pattern. Small, intense localised barium (Ba) inputs, however, cannot be ruled out, as fluctuations in Ba concentration across the coral colonies also suggest sharp and brief Ba-input events. In oceanic corals, upwelling serves as a potential source of pulsed Ba input, associated with increased local productivity and sedimentation of particulates and planktonic tests. Periodic upwelling from April to October has been observed further down the western Greenland coast (Juul-Pedersen et al., 2006), and studies on pelagic productivity and food web structure in Disko Bay have documented strong benthic-pelagic coupling with springtime blooms (Heide-Jørgensen et al., 2007) and the prevalence of large calanoid copepods, bacterioplankton, and unicellular zooplankton (Nielsen and Hansen, 1995; Nielsen and Hansen, 1999; Hansen et al., 2003). However, caution must be exercised when using barium as a benthic-pelagic tracer in the Arctic, as previous research indicates non-conservative behaviour even during low biological productivity periods, likely due to sea-ice microenvironment processes (Hendry et al., 2018). Coral spawning, which significantly affects coral physiology (Gagan et al., 1994; Gagan et al., 1996), may also contribute to the anomalous Ba peaks via a vital effect. Tracey et al. (2007) suggest that reproduction can influence the element composition in bamboo corals, and the existence of an annual reproductive cycle in a lower-latitude Canadian bamboo coral (*Keratoisis ornata*; Mercier and Hamel, 2011) provides an alternative explanation for the synchronous annual Ba concentration cycles between colonies. While the influence of temperature on spawning has been observed in tropical corals (*Montastraea annularis*; Mendes and Woodley, 2002), and is known to influence reproductive strategy in deep-water octocorals (Rakka et al., 2021; Larkin et al., 2023), the role of temperature has not been specifically investigated in *Keratoisis* spp. If any climate-driven environmental variables also affect

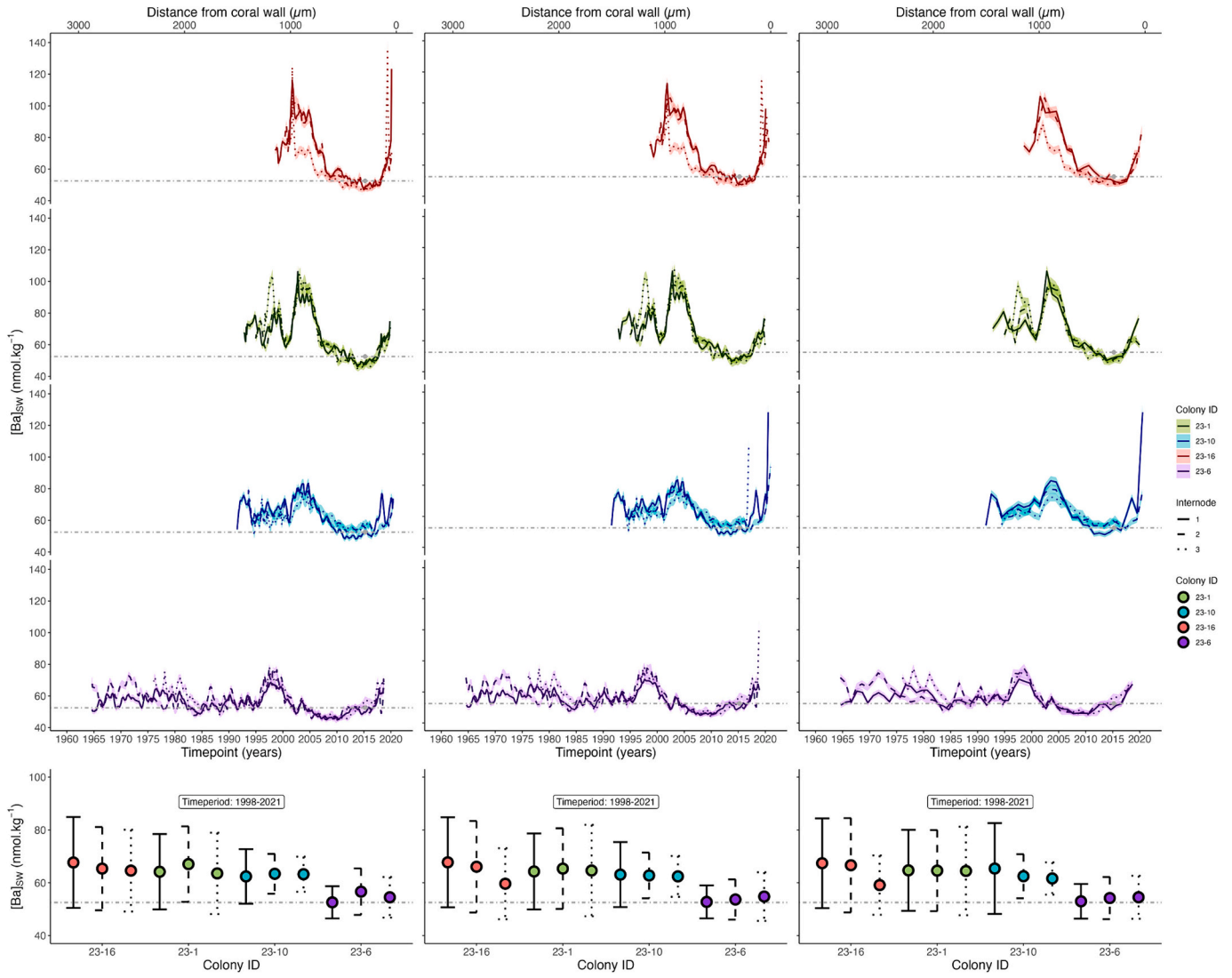

Fig. 5. (*continued*).

spawning in this context, it would further complicate the application of barium as a nutrient tracer. Nonetheless, the clearly correlated trends in Ba/Ca seen within and between individuals strongly suggests that Ba/Ca has considerable potential as an environmental or physiological tracer in *Keratoisis* sp. skeletons.

5. Conclusions and outlook

The micrometre-scale analysis of the chemical composition of deep-sea bamboo coral, *Keratoisis* sp., reveals significant ontogenetic variability in Mg/Ca and Ba/Ca within and among individuals of the species, suggesting the interpretation of raw signals should proceed with caution as the levels of variation are larger than those predicted from records of environmental variation. Replicate transects and colony-specific calibrations improve the reliability of geochemical records and help differentiate true paleoenvironmental variation from ontogenetic discrepancies, whilst elemental mapping allows better choice of representative sections relative to that achieved using bulk analyses or point/line scans. At the microscale, distinct geochemical features are observed in the *Keratoisis* sp. skeletons, with a high-density skeletal layer located near the central axis and a less dense layer lining the outer edge of the internode. Mg/Ca and Li/Ca covary positively within the skeletal structure, while Sr/Ca and U/Ca exhibit a weak negative covariance. Ba/Ca shows significant banding across each internode. The central portion of the internode is deemed the most suitable location for paleoenvironmental reconstruction due to the existence of a potential two-stage calcification process influencing the outer coral edge and faster calcification near the central axis. Careful selection of representative sections is necessary to minimise vital effects and enhance the statistical precision of climate reconstructions.

In the deep-water basin of Baffin Bay, *Keratoisis* sp. plays a crucial role in forming habitat and supporting benthic functioning (Pierrejean et al., 2020), and previous studies have highlighted the significant and lasting influence of palaeoclimate on biodiversity dynamics, including contemporary spatial patterns (Svenning et al., 2015). As the latter are poorly constrained, it would be beneficial for future investigations to prioritise elucidating the intricate dynamics between oceanographic conditions and proximate functioning. Nevertheless, despite uncertainties stemming from taxonomic-derived age models and ontogenetic variability among *Keratoisis* sp. colonies, our application of the Octocoral Mg/Ca proxy reveals a gradual cooling trend over the past 20 years and a 20th-century warming trend in the longest-lived coral, which is in good agreement with available in-situ records. While our findings suggest limited evidence of temperature influencing Ba uptake, which exhibits a nutrient-like profile in open oceans and tracks the patterns of other algal nutrients (Chow and Goldberg, 1960; Wolgemuth

Table 6
Temperature trends (negative indicative of cooling, positive indicative of warming) for Mg/Ca-T reconstruction between time period common to *Keratoisis* sp. colonies (2003–2016) obtained from Ordinary Least Squares (OLS) and Reduced Major Axis (RMA) regressions on un-interpolated, seasonally interpolated and annual interpolated temperature data. Significant regressions are highlighted in bold.

Relationship	x unit	y unit	Interpolation	Colony ID	Internode	n	r	r2	Regression Type	p	Gradient	± 2SD
Temperature ~ Time	Year	°C	Un-interpolated	#23–1	1	130	**−0.22**	**0.0**	**OLS**	**0.007**	**−0.02**	**0.02**
						130	**−0.22**	**0.0**	**RMA**	**0.007**	**−0.06**	**0.05**
					2	140	**−0.40**	**0.2**	**OLS**	**0.001**	**−0.04**	**0.02**
						140	**−0.40**	**0.2**	**RMA**	**0.001**	**−0.08**	**0.03**
					3	132	−0.04	0.0	OLS	0.315	0.00	0.02
						132	−0.04	0.0	RMA	0.315	−0.01	0.05
				#23–10	1	130	**−0.69**	**0.5**	**OLS**	**0.001**	**−0.16**	**0.03**
						130	**−0.69**	**0.5**	**RMA**	**0.001**	**−0.23**	**0.05**
					2	101	**−0.70**	**0.5**	**OLS**	**0.001**	**−0.17**	**0.03**
						101	**−0.70**	**0.5**	**RMA**	**0.001**	**−0.24**	**0.05**
					3	91	**−0.74**	**0.5**	**OLS**	**0.001**	**−0.22**	**0.04**
						91	**−0.74**	**0.5**	**RMA**	**0.001**	**−0.29**	**0.06**
				#23–16	1	132	−0.15	0.0	OLS	0.051	−0.02	0.02
						132	−0.15	0.0	RMA	0.051	−0.04	0.04
					2	109	0.02	0.0	OLS	0.415	0.00	0.03
						109	0.02	0.0	RMA	0.415	0.00	0.05
					3	78	−0.17	0.0	OLS	0.064	−0.04	0.05
						78	−0.17	0.0	RMA	0.064	−0.08	0.13
				#23–6	1	129	−0.04	0.0	OLS	0.308	0.00	0.01
						129	−0.04	0.0	RMA	0.308	−0.01	0.04
					2	176	**0.25**	**0.1**	**OLS**	**0.001**	**0.02**	**0.01**
						176	**0.25**	**0.1**	**RMA**	**0.001**	**0.02**	**0.01**
					3	116	0.03	0.0	OLS	0.383	0.00	0.02
						116	0.03	0.0	RMA	0.383	0.01	0.05
			Seasonal	#23–1	1	52	−0.21	0.0	OLS	0.071	−0.02	0.03
						52	−0.21	0.0	RMA	0.071	−0.07	0.15
					2	52	**−0.46**	**0.2**	**OLS**	**0.001**	**−0.05**	**0.02**
						52	**−0.46**	**0.2**	**RMA**	**0.001**	**−0.08**	**0.05**
					3	52	−0.01	0.0	OLS	0.462	0.00	0.03
						52	−0.01	0.0	RMA	0.462	0.00	0.14
				#23–10	1	52	**−0.69**	**0.5**	**OLS**	**0.001**	**−0.16**	**0.05**
						52	**−0.69**	**0.5**	**RMA**	**0.001**	**−0.23**	**0.08**
					2	52	**−0.71**	**0.5**	**OLS**	**0.001**	**−0.17**	**0.05**
						52	**−0.71**	**0.5**	**RMA**	**0.001**	**−0.23**	**0.07**
					3	52	**−0.79**	**0.6**	**OLS**	**0.001**	**−0.29**	**0.06**
						52	**−0.79**	**0.6**	**RMA**	**0.001**	**−0.38**	**0.09**
				#23–16	1	52	−0.13	0.0	OLS	0.184	−0.02	0.04
						52	−0.13	0.0	RMA	0.184	−0.03	0.07
					2	48	−0.04	0.0	OLS	0.415	−0.01	0.05
						48	−0.04	0.0	RMA	0.415	−0.02	0.18
					3	48	−0.13	0.0	OLS	0.176	−0.03	0.07
						48	−0.13	0.0	RMA	0.176	−0.07	0.20
				#23–6	1	52	−0.02	0.0	OLS	0.431	0.00	0.02
						52	−0.02	0.0	RMA	0.431	−0.01	–
					2	52	0.22	0.0	OLS	0.055	0.02	0.02
						52	0.22	0.0	RMA	0.055	0.04	0.05
					3	52	0.02	0.0	OLS	0.445	0.00	0.03
						52	0.02	0.0	RMA	0.445	0.01	0.25
			Annual	#23–1	1	20	−0.35	0.1	OLS	0.07	−0.04	0.05
						20	−0.35	0.1	RMA	0.07	−0.06	0.11
					2	21	**−0.50**	**0.3**	**OLS**	**0.01**	**−0.05**	**0.04**
						21	**−0.50**	**0.3**	**RMA**	**0.01**	**−0.08**	**0.10**
					3	20	−0.17	0.0	OLS	0.213	−0.01	0.04
						20	−0.17	0.0	RMA	0.213	−0.06	NA
				#23–10	1	21	**−0.71**	**0.5**	**OLS**	**0.001**	**−0.20**	**0.09**
						21	**−0.71**	**0.5**	**RMA**	**0.001**	**−0.24**	**0.14**
					2	21	**−0.84**	**0.7**	**OLS**	**0.001**	**−0.17**	**0.05**
						21	**−0.84**	**0.7**	**RMA**	**0.001**	**−0.20**	**0.07**
					3	17	**−0.64**	**0.4**	**OLS**	**0.008**	**−0.17**	**0.12**
						17	**−0.64**	**0.4**	**RMA**	**0.008**	**−0.27**	**0.29**
				#23–16	1	19	**−0.74**	**0.6**	**OLS**	**0.001**	**−0.13**	**0.06**
						19	**−0.74**	**0.6**	**RMA**	**0.001**	**−0.16**	**0.09**
					2	17	**−0.65**	**0.4**	**OLS**	**0.002**	**−0.19**	**0.12**
						17	**−0.65**	**0.4**	**RMA**	**0.002**	**−0.25**	**0.20**
					3	17	**−0.55**	**0.3**	**OLS**	**0.013**	**−0.12**	**0.10**
						17	**−0.55**	**0.3**	**RMA**	**0.013**	**−0.16**	**0.18**
				#23–6	1	19	**−0.44**	**0.2**	**OLS**	**0.037**	**−0.04**	**0.04**
						19	**−0.44**	**0.2**	**RMA**	**0.037**	**−0.06**	**0.10**
					2	19	−0.05	0.0	OLS	0.44	0.00	0.04
						19	−0.05	0.0	RMA	0.44	−0.01	0.10
					3	19	**−0.53**	**0.3**	**OLS**	**0.009**	**−0.06**	**0.05**
						19	**−0.53**	**0.3**	**RMA**	**0.009**	**−0.10**	**0.12**

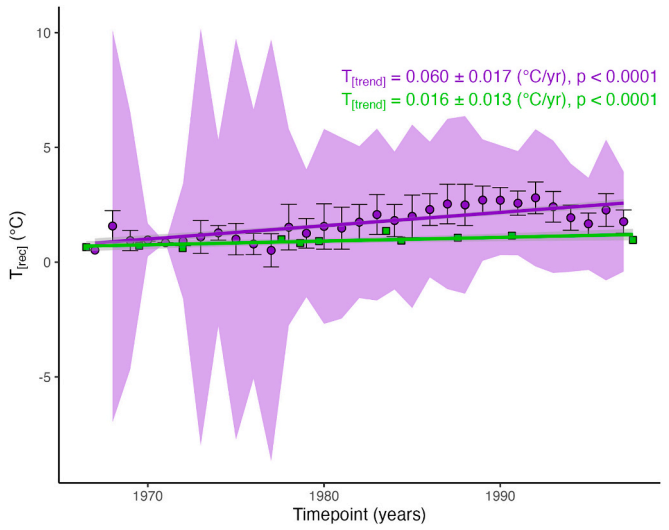

Fig. 6. In-situ temperature data (**green squares**) and trend (**green line**, shaded area is standard error of Ordinary Least Squares regression) for Baffin Bay (Zweng and Münchow, 2006) vs annually interpolated reconstructed temperature data (**purple circles**, error bars denote standard error after averaging across internodes), trend (**purple line**, grey shaded area is standard error of Ordinary Least Squares regression) and confidence belts (**purple shaded area,** 95% confidence intervals after averaging across internodes) in *Keratoisis* sp. colony #23–6. Note the confidence belt constraining once the third internode begins in 1978. (For interpretation of the references to colour in this figure legend, the reader is referred to the web version of this article.)

and Broecker, 1970), the reproducible reconstructions of pronounced and frequent spikes in reconstructed $[Ba]_{SW}$ indicate potential influences from sea-ice, upwelling, phytoplankton blooms, and/or spawning events, which themselves can be affected by climate-driven environmental factors. To enhance confidence in utilising this coral species for deep-water palaeoenvironmental reconstructions, colony-specific growth rates, site-specific calibrations based on in-situ measurements of environmental data, and direct metrics of ecosystem functioning (e.g. sediment oxygen demand and carbon context) need to be incorporated. We contend that such a comprehensive approach will improve the resolution of reconstructed environmental variability and provide insights into the potential influences of temperature and other climate-driven environmental factors on benthic ecosystem functioning.

Declaration of competing interest

The authors declare that they have no known competing financial interests or personal relationships that could have appeared to influence the work reported in this paper.

Data availability

Data used for the research described in the article is included in the tables or electronic supplementary material.

Acknowledgments

This work was undertaken whilst T.J.W. was in receipt of a National Environmental Research Council Funded (INSPIRE) PhD studentship [grant number NE/S007210/1, 2019-2027] with Computed Tomography scanning supported by the National Research Facility for Lab X-ray CT (NXCT) at the μ-VIS X-ray Imaging Centre, University of Southampton [EPSRC grant EP/T02593X/1]. The geochemical analyses were supported by ERC Advanced Grant 884650 Microns2Reefs awarded to G.L.F. T.J.W thanks the Université Laval and ArcticNet for additional financial support to participate in the 2021 Amundsen expedition (Geoffroy et al., 2021). We thank the scientific personnel and crew of the 2021 Amundsen expedition, Keith Tamburri (CSSF-ROPOS), Peter Lockhart (CSSF-ROPOS), Barry Brake (CSSF-ROPOS), Evan Edinger (Memorial University of Newfoundland), Bárbara de Moura Neves (Fisheries and Oceans Canada), and Guillaume Blais (Université Laval) for aiding in the collection and processing of the coral colonies. We gratefully acknowledge Dan Doran (University of Southampton) for sample preparation, Andy Milton (University of Southampton) for analytical support, the Amundsen Science team, Canada for logistical support and we are grateful for the IRIDIS High Performance Computing Facility, University of Southampton. Some of the temperature, salinity and oxygen data presented herein were collected onboard the Canadian research icebreaker CCGS Amundsen and made available by Amundsen Science Inc., which is supported by the Canada Foundation for Innovation. The views expressed in this publication do not necessarily represent the views of Amundsen Science or that of its partners.

Appendix A. Supplementary data

Supplementary data to this article can be found online at https://doi.org/10.1016/j.chemgeo.2024.122053.

References

Adkins, J.F., Cheng, H., Boyle, E.A., Druffel, E.R.M., Edwards, R.L., 1998. Deep-Sea coral evidence for rapid change in ventilation of the deep North Atlantic 15,400 years Ago. Science 280 (5364), 725–728. https://doi.org/10.1126/science.280.5364.725.

Adkins, J.F., Boyle, E.A., Curry, W.B., Lutringer, A., 2003. Stable isotopes in deep-sea corals and a new mechanism for "vital effects". Geochim. Cosmochim. Acta 67 (6), 1129–1143.

Alibert, C., McCulloch, M.T., 1997. Strontium/calcium ratios in modern *Porites* corals from the Great Barrier Reef as a proxy for sea surface temperature: Calibration of the thermometer and monitoring of ENSO. Paleoceanography 12, 345–363.

Alpert, A.E., et al., 2016. Comparison of equatorial Pacific Sea surface temperature variability and trends with Sr/ca records from multiple corals. Paleoceanography 31 (2), 252–265.

Amundsen Science Data Collection, . CTD-Rosette Data Collected by the CCGS Amundsen in the Canadian Arctic and Sub-Arctic. Raw data. Limited Distribution. Accessed from amundsen.data@as.ulaval.ca, on [2021-06-23]. Processed data are archived at. www.polardata.ca. https://doi.org/10.5884/12713.

Anagnostou, E., et al., 2011. Seawater nutrient and carbonate ion concentrations recorded as P/Ca, Ba/Ca, and U/ca in the deep-sea coral *Desmophyllum dianthus*. Geochim. Cosmochim. Acta 75 (9), 2529–2543.

Anagnostou, E., Huang, K.F., You, C.F., Sikes, E.L., Sherrell, R.M., 2012. Evaluation of boron isotope ratio as a pH proxy in the deep sea coral *Desmophyllum dianthus*: evidence of physiological pH adjustment. Earth Planet. Sci. Lett. 349-350, 251–260.

Andrews, A.H., Stone, R.P., Lundstrom, C.C., DeVogelaere, A.P., 2009. Growth rate and age determination of bamboo corals from the Northeastern Pacific Ocean using refined 210Pb dating. Mar. Ecol. Prog. Ser. 397, 173–185.

Aranha, R., Edinger, E., Layne, G., Piercey, G., 2014. Growth rate variation and potential paleoceanographic proxies in *Primnoa pacifica*: Insights from high-resolution trace element microanalysis. Deep-Sea Res. II Top. Stud. Oceanogr. 99, 213–226.

Armid, A., et al., 2011. Seawater temperature proxies based on D_{Sr}, D_{Mg}, and D_U from culture experiments using the branching coral *Porites cylindrica*. Geochim. Cosmochim. Acta 75 (15), 4273–4285.

Auscavitch, S.R., et al., 2020. Distribution of deep-water scleractinian and stylasterid corals across abiotic environmental gradients on three seamounts in the Anegada Passage. PeerJ 8, e9523.

Azetsu-Scott, K., Petrie, B., Yeats, P., Lee, C., 2012. Composition and fluxes of freshwater through Davis Strait using multiple chemical tracers. J. Geophys. Res. Oceans 117 (C12).

Bailey, R.G., 1998. Ecoregions: The Ecosystem Geography of the Oceans and Continents. Springer, New York.

Battaglia, G., Joos, F., 2018. Hazards of decreasing marine oxygen: the near-term and millennial-scale benefits of meeting the Paris climate targets. Earth Syst. Dynam. 9, 797–816. https://doi.org/10.5194/esd-9-797-2018.

Bayer, F.M., 1956. Octocorallia.

Bayer, F.M., Stefani, J., 1987. New and previously known taxa of Isidid Octocorals (Coelenterate: *Gorgonacea*) partly from Antarctic waters. Proc. Biol. Soc. Wash. 100 (4), 937–991.

Birch, J.R., et al., 1983. Arctic data compilation and appraisal volume 5. Baffin Bay: Physical Oceanography - Temperature, Salinity, Currents and Water Levels. In: Institute of Ocean Sciences Department of Fisheries and Oceans, Sidney, B. C.

Bolnick, D.I., et al., 2011. Why intraspecific trait variation matters in community ecology. Trends Ecol. Evol. 26 (4), 183–192.

Buch, E., et al., 2019. Arctic in Situ Data Availability. European Environment Agency.

Case, D.H., Robinson, L.F., Auro, M.E., Gagnon, A.C., 2010. Environmental and biological controls on Mg and Li in deep-sea scleractinian corals. Earth Planet. Sci. Lett. 300 (3–4), 215–225.

Chaabane, S., et al., 2019. Elemental systematics of the calcitic skeleton of *Corallium rubrum* and implications for the Mg/ca temperature proxy. Chem. Geol. 524, 237–258.
Chalk, T.B., et al., 2021. Mapping coral calcification strategies from in situ boron isotope and trace element measurements of the tropical coral Siderastrea siderea. Sci. Rep. 11 (1), 472.
Chen, C.-T.A., et al., 2017. Deep oceans may acidify faster than anticipated due to global warming. Nat. Clim. Chang. 7 (12), 890–894.
Chow, T.J., Goldberg, E.D., 1960. On the marine geochemistry of barium. Geochim. Cosmochim. Acta 20, 192–198.
Cianciaruso, M.V., et al., 2009. Including intraspecific variability in functional diversity. Ecology 90, 81–89. https://doi.org/10.1890/07-1864.1.
Clarke, H., D'Olivo, J.P., Conde, M., Evans, R.D., McCulloch, M.T., 2019. Coral Records of Variable stress Impacts and possible Acclimatization to recent Marine Heat Wave events on the Northwest Shelf of Australia. Paleoceanograph. Paleoclimatol. 34 (11), 1672–1688.
Cobb, G.W., 1998. Introduction to Design and Analysis of Experiments. Springer-Verlag, New York.
Cuny-Guirriec, K., et al., 2019. Coral Li/Mg thermometry: Caveats and constraints. Chem. Geol. 523, 162–178.
Curry, B., Lee, C.M., Petrie, B., 2011. Volume, Freshwater, and Heat Fluxes through Davis Strait, 2004-05. J. Phys. Oceanogr. 41 (3), 429–436.
Davies, A.J., Wisshak, M., Orr, J.C., Murray Roberts, J., 2008. Predicting suitable habitat for the cold-water coral *Lophelia pertusa* (Scleractinia). Deep-Sea Res. I Oceanogr. Res. Pap. 55 (8), 1048–1062.
DeLong, K.L., Quinn, T.M., Taylor, F.W., 2007. Reconstructing twentieth-century sea surface temperature variability in the Southwest Pacific: A replication study using multiple coral Sr/ca records from New Caledonia. Paleoceanography 22 (4).
DeLong, K.L., Flannery, J.A., Maupin, C.R., Poore, R.Z., Quinn, T.M., 2011. A coral Sr/ca calibration and replication study of two massive corals from the Gulf of Mexico. Palaeogeogr. Palaeoclimatol. Palaeoecol. 307 (1–4), 117–128.
Farmer, J.R., Hönisch, B., Robinson, L.F., Hill, T.M., 2015a. Effects of seawater-pH and biomineralization on the boron isotopic composition of deep-sea bamboo corals. Geochim. Cosmochim. Acta 155, 86–106.
Farmer, J.R., Robinson, L.F., Honisch, B., 2015b. Growth rate determinations from radiocarbon in bamboo corals (genus *Keratoisis*). In: Deep-Sea Research Part I-Oceanographic Research Papers, 105, pp. 26–40.
Feely, R.A., et al., 2002. In situ calcium carbonate dissolution in the Pacific Ocean. Global Biogeochemical Cycles 16 (4), 91-1-91-12.
Flöter, S.B., 2019. The Potential of Bamboo Corals to Record Environmental Conditions in their Calcitic Skeletons. Christian-Albrechts-Universität.
Flöter, S., et al., 2019. The influence of skeletal micro-structures on potential proxy records in a bamboo coral. Geochim. Cosmochim. Acta 248, 43–60.
Flöter, S., Fietzke, J., Gutjahr, M., Nehrke, G., Eisenhauer, A., 2022. Incorporation of Na and S in bamboo coral skeletons. Chem. Geol. 597.
Frank, N., et al., 2004. Eastern North Atlantic deep-sea corals: tracing upper intermediate water Δ14C during the Holocene. Earth Planet. Sci. Lett. 219 (3–4), 297–309.
Frenkel, M.M., et al., 2017. Quantifying bamboo coral growth rate nonlinearity with the radiocarbon bomb spike: A new model for paleoceanographic chronology development. Deep-Sea Res. Part I-Oceanograph. Res. Paper. 125, 26–39.
Gagan, M.K., Chivas, A.R., Isdale, P.J., 1994. High-resolution isotopic records from corals using ocean temperature and mass-spawning chronometers. Earth Planet. Sci. Lett. 121, 549–558.
Gagan, M.K., Chivas, A.R., Isdale, P.J., 1996. Timing coral-based climatic histories using 13C enrichments driven by synchronized spawning. Geology 24 (11), 1009–1012.
Gagnon, A.C., et al., 2007. Sr/ca and Mg/ca vital effects correlated with skeletal architecture in a scleractinian deep-sea coral and the role of Rayleigh fractionation. Earth Planet. Sci. Lett. 261 (1–2), 280–295.
Garnier, S., et al., 2021. Rvision - Colorblind-Friendly Color Maps for R. R Package Version 0.6.2.
Geoffroy, M., et al., 2021. Leg 2 - Labrador Sea. Davis Strait and Baffin Bay, Amundsen Science.
GEOTRACES Intermediate Data Product Group, 2021. The GEOTRACES Intermediate Data Product 2021 (IDP2021). NERC EDS British Oceanographic Data Centre NOC. https://doi.org/10.5285/cf2d9ba9-d51d-3b7c-e053-8486abc0f5fd.
Geyman, B.M., et al., 2019. Barium in deep-sea bamboo corals: phase associations, barium stable isotopes, & prospects for paleoceanography. Earth Planet. Sci. Lett. 525.
Gonneea, M.E., et al., 2017. Relationship between water and aragonite barium concentrations in aquaria reared juvenile corals. Geochim. Cosmochim. Acta 209, 123–134. https://doi.org/10.1016/j.gca.2017.04.006.
Hansen, A.S., et al., 2003. Impact of changing ice cover on pelagic productivity and food web structure in Disko Bay, West Greenland: a dynamic model approach. Deep-Sea Res. Part I-Oceanograph. Res. Paper. 50 (1), 171–187.
Hathorne, E.C., et al., 2013. Interlaboratory study for coral Sr/ca and other element/ca ratio measurements. Geochem. Geophys. Geosyst. 14, 3730–3750. https://doi.org/10.1002/ggge.20230.
Heide-Jørgensen, M.P., et al., 2007. Springtime coupling between chlorophyll a, sea ice and sea surface temperature in Disko Bay, West Greenland. Prog. Oceanogr. 73 (1), 79–95.
Heikoop, J., et al., 2002. Potential climate signals from the deep-sea gorgonian coral *Primnoa resedaeformis*. Hydrobiologia 471, 117–124. https://doi.org/10.1023/A:1016505421115.
Hendry, K.R., et al., 2018. Spatiotemporal Variability of Barium in Arctic Sea-Ice and Seawater. J. Geophys. Res. Oceans 123 (5), 3507–3522.
Hetzinger, S., Halfar, J., Fronz, A., Simon, K., Adey, W.H., Steneck, R.S., 2018. Reproducibility of *Clathromorphum compactum* coralline algal Mg/Ca ratios and comparison to high-resolution sea surface temperature data. Geochim. Cosmochim. Acta. https://doi.org/10.1016/j.gca.2017.09.044.
Hijmans, R., 2022. terra: Spatial Data Analysis. R Package Version 1.6–47. https://CRAN.R-project.org/package=terra.
Hill, T.M., et al., 2011. Temperature and vital effect controls on bamboo coral (*Isididae*) isotope geochemistry: A test of the "lines method". Geochem. Geophys. Geosyst. 12 (4).
Hill, T.M., et al., 2012. Variations in seawater Sr/ca recorded in deep-sea bamboo corals. Paleoceanography 27 (3).
Hu, M., Chen, T., Zhang, W., 2018. Inter-species and inter-colony differences of Sr/Ca-SST calibration in *Porites*. J. Trop. Oceanogr. 37 (6), 74–84.
Jochum, K.P., et al., 2011. Determination of Reference Values for NIST SRM 610-617 Glasses following ISO guidelines. Geostand. Geoanal. Res. 35 (4), 397–429.
Johannes, R.E., Wiebe, W.J., 1970. Method for Determination of Coral Tissue Biomass and Composition.
Juul-Pedersen, T., et al., 2006. Sedimentation following the spring bloom in Disko Bay, West Greenland, with special emphasis on the role of copepods. Mar. Ecol. Prog. Ser. 314, 239–255.
Kamenos, N.A., Cusack, M., Moore, P.G., 2008. Coralline algae are global paleothermometers with bi-weekly resolution. Geochim. Cosmochim. Acta. https://doi.org/10.1016/j.gca.2007.11.019.
Kawakubo, Y., et al., 2014. Precise determination of Sr/ca by laser ablation ICP-MS compared to ICP-AES and application to multi-century temperate corals. Geochem. J. 48 (2), 145–152.
Kershaw, J., et al., 2023. Ba/Ca of stylasterid coral skeletons records dissolved seawater barium concentrations. Chem. Geol. 622, 121355.
Kimball, J.B., Dunbar, R.B., Guilderson, T.P., 2014. Oxygen and carbon isotope fractionation in calcitic deep-sea corals: Implications for paleotemperature reconstruction. Chem. Geol. 381, 223–233.
Koslow, J.A., et al., 2001. Seamount benthic macrofauna off southern Tasmania: community structure and impacts of trawling. Mar. Ecol. Prog. Ser. 213, 111–125.
Kotov, S., Pälike, H., 2018. QAnalySeries – A Cross-Platform Time Series Tuning and Analysis Tool. AGU, Washington. https://doi.org/10.1002/essoar.10500226.1.
Laidre, K.L., et al., 2020. Interrelated ecological impacts of climate change on an apex predator. Ecol. Appl. 30 (4), e02071.
Larkin, M.F., Davis, T.R., Harasti, D., Smith, S.D.A., Ainsworth, T.D., Benkendorff, K., 2023. A glimmer of hope for an Endangered temperate soft coral: the first observations of reproductive strategies and early life cycle of *Dendronephthya australis* (Octocorallia: Malacalcyonacea). Mar. Biol. 170 (11) https://doi.org/10.1007/s00227-023-04298-x.
LaVigne, M., Hill, T.M., Spero, H.J., Guilderson, T.P., 2011. Bamboo coral Ba/ca: Calibration of a new deep ocean refractory nutrient proxy. Earth Planet. Sci. Lett. 312 (3–4), 506–515.
Lazareth, C.E., et al., 2016. Intra-skeletal calcite in a live-collected *Porites* sp.: Impact on environmental proxies and potential formation process. Geochim. Cosmochim. Acta 176, 279–294.
Legendre, P., 2018. model2: Model II Regression. R Package Version 1.7–3. https://CRAN.R-project.org/package=lmodel2.
Levin, L.A., Le Bris, N., 2015. The deep ocean under climate change. Science 350 (6262), 766–768.
Lopez Correa, M., Montagna, P., Joseph, N., Rüggeberg, A., McCulloch, M., 2011. Geochemical records in Canadian bamboo corals, potentials and pitfalls. Geophys. Res. Abstr. 13. EGU2011-13944.
Lutringer, A., Blamart, D., Frank, N., Labeyrie, L., 2005. Paleotemperatures from deep-sea corals: Scale effects. In: Freiwald, A., Roberts, J.M. (Eds.), Cold-Water Corals and Ecosystems. Springer, pp. 631–640.
Mankoff, K.D., et al., 2020. Greenland Ice Sheet solid ice discharge from 1986 through March 2020. Earth Sys. Sci. Data 12 (2), 1367–1383.
McFadden, C.S., Cordeiro, R., Williams, G., van Ofwegen, L., 2023. World List of Octocorallia. Keratoisididae Gray, 1870. World Register of Marine Species. https://www.marinespecies.org/aphia.php?p=taxdetails&id=1419319 [Accessed on 2023-06-13].
Mendes, J.M., Woodley, J.D., 2002. Timing of reproduction in *Montastraea annularis* : relationship to environmental variables. Mar. Ecol. Prog. Ser. 227, 241–251.
Mercier, A., Hamel, J.F., 2011. Contrasting reproductive strategies in three deep-sea Octocorals from eastern Canada: *Primnoa resedaeformis*, *Keratoisis ornata*, and *Anthomastus grandiflorus*. Coral Reefs 30, 337–350.
Montagna, P., McCulloch, M., Taviani, M., Remia, A., Rouse, G., 2005. High-resolution trace and minor element compositions in deep-water scleractinian corals (*Desmophyllum dianthus*) from the Mediterranean Sea and the Great Australian Bight. In: Freiwald, A., Roberts, J.M. (Eds.), Cold-Water Corals and Ecosystems. Springer, pp. 1109–1126.
Montagna, P., et al., 2014. Li/Mg systematics in scleractinian corals: Calibration of the thermometer. Geochim. Cosmochim. Acta 132, 288–310.
Neves, B.D.M., et al., 2014. Deep-water bamboo coral forests in a muddy Arctic environment. Mar. Biodivers. 45 (4), 867–871.
Nielsen, T.G., Hansen, B.W., 1995. Plankton community structure and carbon cycling on the western coast of Greenland during and after the sedimentation of a diatom bloom. Mar. Ecol. Prog. Ser. 125, 239–257.
Nielsen, T.G., Hansen, B.W., 1999. Plankton community structure and carbon cycling on the western coast of Greenland during the stratified summer situation. I. Hydrography, phytoplankton and bacterioplankton. Aquat. Microb. Ecol. 16, 205–216.

Noé, S.U., Dullo, W.C., 2006. Skeletal morphogenesis and growth mode of modern and fossil deep-water isidid gorgonians (Octocorallia) in the West Pacific (New Zealand and Sea of Okhotsk). Coral Reefs 25 (3), 303–320.
Noé, S.U., Lembke-Jene, L., Dullo, W.C., 2008. Varying growth rates in bamboo corals: sclerochronology and radiocarbon dating of a mid-Holocene deep-water gorgonian skeleton (*Keratoisis* sp.: Octocorallia) from Chatham rise (New Zealand). Facies 54 (2), 151–166.
Nozaki, Y., 1997. A fresh look at element distribution in the North Pacific Ocean. In: Eos Transactions American Geophysical Union, 78, p. 221.
Nusbaumer, J., Alexander, P.M., LeGrande, A.N., Tedesco, M., 2019. Spatial Shift of Greenland Moisture sources Related to Enhanced Arctic Warming. Geophys. Res. Lett. 46 (24), 14723–14731.
Ó Cofaigh, C., et al., 2018. The role of meltwater in high-latitude trough-mouth fan development: The Disko Trough-Mouth Fan, West Greenland. Mar. Geol. 402, 17–32.
Pedersen, T., 2022. Patchwork: The Composer of Plots. R Package Version 1.1.2. Retrieved from. https://CRAN.R-project.org/package=patchwork.
Pickart, R.S., Torres, D.J., Clarke, R.A., 2002. Hydrography of the Labrador Sea during active convection. J. Phys. Oceanogr. 32, 428–457.
Pickart, R.S., et al., 2003. Deep convection in the Irminger Sea forced by the Greenland tip jet. Nature 424, 152–156.
Pierrejean, M., et al., 2020. Influence of Deep-Water Corals and Sponge Gardens on Infaunal Community Composition and Ecosystem Functioning in the Eastern Canadian Arctic. Front. Mar. Sci. 7.
Pinheiro, J., Bates, D.M., 2000. Mixed-Effects Models in S and S-PLUS. Statistics and Computing. Springer.
Pinheiro, J., Bates, D., R Core Team, 2022. Nlme: Linear and Nonlinear Mixed Effects Models. R Package Version 3.1–160. Retrieved from. https://CRAN.R-project.org/package=nlme.
Pistevos, J.C.A., Calosi, P., Widdicombe, S., Bishop, J.D.D., 2011. Will variation among genetic individuals influence species responses to global climate change? Oikos 120, 675–689.
Quinn, T.M., Sampson, D.E., 2002. A multiproxy approach to reconstructing sea surface conditions using coral skeleton geochemistry. Paleoceanography 17 (4), 11.
R Core Team, 2022. R: A Language and Environment for Statistical Computing. R Foundation for Statistical Computing. Retrieved from. https://www.R-project.org/.
Rakka, M., Sampaio, Í., Colaço, A., Carreiro-Silva, M., 2021. Reproductive biology of two deep-sea octocorals in the Azores Archipelago. Deep-Sea Res. I Oceanogr. Res. Pap. 175, 103587 https://doi.org/10.1016/j.dsr.2021.103587.
Reynolds, R.W., et al., 2002. An improved in situ and satellite SST analysis for climate. J. Clim. 15, 1609–1625.
Roark, B.E., et al., 2005. Radiocarbon based ages and growth rates of bamboo corals from the Gulf of Alaska. Geophys. Res. Lett. 32, LO4606.
Robinson, L.F., et al., 2005. Radiocarbon Variability in the Western North Atlantic during the last Deglaciation. Science 310 (5753), 1469–1473.
Robinson, L.F., et al., 2014. The geochemistry of deep-sea coral skeletons: A review of vital effects and applications for paleoceanography. Deep-Sea Res. II Top. Stud. Oceanogr. 99, 184–198.
Rogers, A.D., 1999. The Biology of *Lophelia pertusa* (Linnaeus 1758) and Other Deep-Water Reef-Forming Corals and Impacts from Human Activities. Int. Rev. Hydrobiol. 84 (4), 315–406.
Rogers, A.D., 2015. Environmental Change in the Deep Ocean. Annu. Rev. Environ. Resour. 40 (1), 1–38.
Rohatgi, A., 2022. WebPlotDigitizer (Version 4.6) [Computer Software]. Retrieved from. http://arohatgi.info/WebPlotDigitizerRoss.
Ross, C.L., DeCarlo, T.M., McCulloch, M.T., 2019. Calibration of Sr/Ca, Li/Mg and Sr-U Paleothermometry in Branching and Foliose Corals. Paleoceanograph. Paleoclimatol. 34 (8), 1271–1291.
Schlegel, P., Havenhand, J.N., Gillings, M.R., Williamson, J.E., 2012. Individual variability in reproductive success determines winners and losers under ocean acidification: A case study with sea urchins. PLoS One 7, e53118. https://doi.org/10.1371/journal.pone.0053118.
Schloerke, B., et al., 2021. GGally: Extension to 'ggplot2'. R Package Version 2.1.2. https://CRAN.R-project.org/package=GGally.
Sherwood, O.A., Edinger, E.N., 2009. Ages and growth rates of some deep-sea gorgonian and antipatharian corals of Newfoundland and Labrador. Can. J. Fish. Aquat. Sci. 66 (1), 142–152.
Sherwood, O.A., Risk, M.J., 2007. Chapter twelve Deep-Sea Corals: New Insights to Paleoceanography. In: Proxies in late Cenozoic Paleoceanography. Developments in Marine Geology, pp. 491–522.
Sherwood, O.A., et al., 2005a. Stable isotopic composition of deep-sea gorgonian corals *Primnoa* spp.: a new archive of surface processes. Mar. Ecol. Prog. Ser. 301, 135–148. https://doi.org/10.3354/meps301135.
Sherwood, O.A., et al., 2005b. Skeletal Mg/ca in *Primnoa resedaeformis*: Relationship to temperature? In: Freiwald, A., Roberts, J.M. (Eds.), Cold-Water Corals and Ecosystems. Springer, pp. 389–398.
Sherwood, O.A., et al., 2008. Late Holocene radiocarbon variability in Northwest Atlantic slope waters. Earth Planet. Sci. Lett. 275 (1–2), 146–153.
Sherwood, O.A., Lehmann, M.F., Schubert, C.J., Scott, D.B., McCarthy, M.D., 2011. Nutrient regime shift in the western North Atlantic indicated by compound-specific N of deep-sea gorgonian corals. Proc. Natl. Acad. Sci. 108 (3), 1011–1015.
Sinclair, D.J., McCulloch, M.T., 2004. Corals record low mobile barium concentrations in the Burdekin River during the 1974 flood: evidence for limited Ba supply to rivers? Palaeogeogr. Palaeoclimatol. Palaeoecol. 214, 155–174.
Sinclair, D.J., et al., 2011. Reproducibility of trace element profiles in a specimen of the deep-water bamboo coral *Keratoisis* sp. Geochim. Cosmochim. Acta 75 (18), 5101–5121.
Sinclair, D.J., Williams, B., Risk, M., 2006. A biological origin for climate signals in corals — Trace element "vital effects" are ubiquitous in Scleractinian coral skeletons. Geophys. Res. Lett. https://doi.org/10.1029/2006gl027183.
Smith, J.E., et al., 2000. Paleotemperatures from deep-sea corals: Overcoming 'vital effects'. PALAIOS 15 (1), 25–32.
Smith, G.C., et al., 2019. Polar Ocean Observations: A critical Gap in the observing System and its effect on Environmental predictions from hours to a season. Front. Mar. Sci. 6.
Spalding, M.D., et al., 2007. Marine ecoregions of the world: a bioregionalization of coastal and shelf areas. Bioscience 57, 573–583.
Spiess, A.-N., Neumeyer, N., 2010. An evaluation of R^2 as an inadequate measure for nonlinear models in pharmacological and biochemical research: a Monte Carlo approach. BMC Pharmacol. 10 (6).
Spooner, P.T., et al., 2018. Extended calibration of cold-water coral Ba/ca using multiple genera and co-located measurements of dissolved barium concentration. Chem. Geol. 499, 100–110. https://doi.org/10.1016/j.chemgeo.2018.09.012.
Standish, C.D., et al., 2019. The effect of matrix interferences on in situ boron isotope analysis by laser ablation multi-collector inductively coupled plasma mass spectrometry. Rapid Commun. Mass Spectrom. 33, 959–968.
Stewart, J.A., Anagnostou, E., Foster, G.L., 2016. An improved boron isotope pH proxy calibration for the deep-sea coral *Desmophyllum dianthus* through sub-sampling of fibrous aragonite. Chem. Geol. 447, 148–160.
Stewart, J.A., et al., 2020. Refining trace metal temperature proxies in cold-water scleractinian and stylasterid corals. Earth Planet. Sci. Lett. 545.
Stewart, J.A., Strawson, I., Kershaw, J., Robinson, L.F., 2022. Stylasterid corals build aragonite skeletons in undersaturated water despite low pH at the site of calcification. Sci. Rep. 12 (1), 13105.
Svenning, J.-C., Eiserhardt, W.L., Normand, S., Ordonez, A., Sandel, B., 2015. The Influence of Paleoclimate on Present-Day patterns in Biodiversity and Ecosystems. Annu. Rev. Ecol. Evol. Syst. 46 (1), 551–572.
Sweetman, A.K., et al., 2017. Major impacts of climate change on deep-sea benthic ecosystems. Element.: Sci. Anthropocene 5, 1–23.
Thomas, H., et al., 2021. Inorganic carbon, Ra, Ba and, δ18O tracer distribution in the Canadian Arctic Archipelago from the 2015 Canadian GEOTRACES expedition. PANGAEA. https://doi.org/10.1594/PANGAEA.929298.
Thresher, R.E., Neil, H., 2016. Scale dependence of environmental and physiological correlates of δ18O and δ13C in the magnesium calcite skeletons of bamboo corals (Gorgonacea; *Isididae*). Geochim. Cosmochim. Acta 187, 260–278.
Thresher, R.E., et al., 2004. Oceanic evidence of climate change in southern Australia over the last three centuries. Geophys. Res. Lett. 31, L07212. https://doi.org/10.1029/2003GL018869.
Thresher, R.E., et al., 2009. Environmental and compositional correlates of growth rate in deep-water bamboo corals (Gorgonacea; *Isididae*). Mar. Ecol. Prog. Ser. 397, 187–196.
Thresher, R.E., Wilson, N.C., MacRae, C.M., Neil, H., 2010. Temperature effects on the calcite skeletal composition of deep-water gorgonians (*Isididae*). Geochim. Cosmochim. Acta 74 (16), 4655–4670.
Thresher, R.E., Fallon, S.J., Townsend, A.T., 2016. A "core-top" screen for trace element proxies of environmental conditions and growth rates in the calcite skeletons of bamboo corals (*Isididae*). Geochim. Cosmochim. Acta 193, 75–99.
Tracey, H., et al., 2007. Age and growth of two genera of deep-sea bamboo corals (Family *Isididae*). In: New Zealand Waters.
Watling, L., Saucier, E.H., France, S.C., 2022. Towards a revision of the bamboo corals (Octocorallia): part 4, delineating the family *Keratoisididae*. Zootaxa 5093 (3), 337–375. https://doi.org/10.11646/zootaxa.5093.3.4.
Weinbauer, M.G., Velimirov, B., 1995. Morphological Variations in the Mediterranean-Sea Fan Eunicella-Cavolini (Coelenterata, Gorgonacea) in Relation to Exposure, Colony size and Colony Region. Bull. Mar. Sci. 56 (1), 283–295.
Weinbauer, M.G., Brandstatter, F., Velimirov, B., 2000. On the potential use of magnesium and strontium concentrations as ecological indicators in the calcite skeleton of the red coral (*Corallium rubrum*). Mar. Biol. 137, 801–809.
West, B., Welch, K., Gałecki, A., 2014. Linear Mixed Models, 2nd ed. https://doi.org/10.1201/b17198-2
Wickham, H., et al., 2019. Welcome to the tidyverse. J. Open Source Softw. 4 (43), 1686. https://doi.org/10.21105/joss.01686.
Williams, T.J. Three-dimensional reconstruction of high latitude bamboo coral via x-ray microfocus computed tomography Sci. Data. (In review).
Wolgemuth, K., Broecker, W.S., 1970. Barium in Sea Water. Earth Planet. Sci. Lett. 8, 372–378.
Zuur, A.F., et al., 2009. Mixed Effects Modelling for Nested Data. In: Zuur, A.F., et al. (Eds.), Mixed Effects Models and Extensions in Ecology with R. Springer, New York, New York, NY, pp. 101–142.
Zuur, A.F., Ieno, E.N., Elphick, C.S., 2010. A protocol for data exploration to avoid common statistical problems. Methods Ecol. Evol. 1 (1), 3–14. https://doi.org/10.1111/j.2041-210x.2009.00001.x.
Zweng, M.M., Münchow, A., 2006. Warming and freshening of Baffin Bay, 1916–2003. J. Geophys. Res. 111 (C7).